REPORT DOCUMENTATION PAGE

AFRL-SR-BL-TR-98-

88

◯ʒʒｌ

g data sources,
r aspect of this
1215 Jefferson
3.

1. AGENCY USE ONLY (Leave blank)	2. REPORT DATE Mar. 1998	3. REPORT TYPE AND DATES COVERED Final Technical Report, Apr 1997-Dec 1997

4. TITLE AND SUBTITLE	5. FUNDING NUMBERS
Automatic Target Recognition using High-Range Resolution data	F49620-97-1-0157

6. AUTHOR(S)
Dr. Arnab K. Shaw

7. PERFORMING ORGANIZATION NAME(S) AND ADDRESS(ES)	8. PERFORMING ORGANIZATION REPORT NUMBER
Wright State University, Dayton, OH 45435	Ohio TR-1

9. SPONSORING/MONITORING AGENCY NAME(S) AND ADDRESS(ES)	10. SPONSORING/MONITORING AGENCY REPORT NUMBER
Air Force Office of Scientific Research/NM 110 Duncan Avenue, Suite B115 Bolling AFB, DC 20332	

19980511 071

11. SUPPLEMENTARY NOTES

12a. DISTRIBUTION/AVAILABILITY STATEMENT	12b. DISTRIBUTION CODE
Distribution Unlimited	

13. ABSTRACT (Maximum 200 words)

A new algorithm is presented for Automatic Target Recognition (ATR) using High Range Resolution (HRR) profiles as opposed to traditional Synthetic Aperture Radar (SAR) images. ATR performance using SAR images degrades considerably in case of moving targets due to blurring caused in the cross-range domain. ATR based on HRR profiles, which are formed without Fourier transform in the cross-range, is expected to have superior performance for moving targets with the proposed method. One of the major contributions of this project so far has been the utilization of Eigen-templates as ATR features that are obtained via Singular Value Decomposition (SVD) of HRR profiles. SVD analysis of a large class of HRR data revealed that the Range-space eigenvectors corresponding to the largest singular value accounted for more than 90% of target energy. Hence, it has been proposed that the Range-space Eigen-vectors be used as templates for classification. The effectiveness of data normalization and Gaussianization of profile data in improving classification performance is also studied. With extensive simulation studies it is shown that the proposed Eigen-template based ATR approach provides consistent superior performance with recognition rate reaching 99.5% for the four class XPATCH database.

This research project is being conducted in direct collaboration with the Sensors Directorate's ATR Assessment Branch, Wright Laboratories, Wright-Patt AFB, Dayton, Ohio, where it is being monitored by Dr. Rob Williams. A primary objective of this collaborative effort is to complement and augment various other ongoing research activities being conducted or supported by the Wright Labs ATR research team.

14. SUBJECT TERMS Automatic Target Recognition, Synthetic Aperture Radar, SAR, HRR, High Range Resolution Processing, Eigen-Templates, Feature Extraction, Target Classification, XPATCH, MSTAR, Clutter Removal			15. NUMBER OF PAGES 93
			16. PRICE CODE

17. SECURITY CLASSIFICATION OF REPORT UNCLASSIFIED	18. SECURITY CLASSIFICATION OF THIS PAGE UNCLASSIFIED	19. SECURITY CLASSIFICATION OF ABSTRACT UNCLASSIFIED	20. LIMITATION OF ABSTRACT UL

DTIC QUALITY INSPECTED ⑧

Abstract

A new algorithm is presented for Automatic Target Recognition (ATR) using High Range Resolution (HRR) profiles as opposed to traditional Synthetic Aperture Radar (SAR) images. ATR performance using SAR images degrades considerably in case of moving targets due to blurring caused in the cross-range domain. ATR based on HRR profiles, which are formed without Fourier transform in the cross-range, is expected to have superior performance for moving targets with the proposed method. One of the major contributions of this project so far has been the utilization of Eigen-templates as ATR features that are obtained via Singular Value Decomposition (SVD) of HRR profiles. SVD analysis of a large class of HRR data revealed that the Range-space eigenvectors corresponding to the largest singular value accounted for more than 90% of target energy. Hence, it has been proposed that the Range-space Eigen-vectors be used as templates for classification. The effectiveness of data normalization and Gaussianization of profile data in improving classification performance is also studied. With extensive simulation studies it is shown that the proposed Eigen-template based ATR approach provides consistent superior performance with recognition rate reaching 99.5% for the four class XPATCH database.

This research project is being conducted in direct collaboration with the Sensors Directorate's ATR Assessment Branch, Wright Laboratories, Wright-Patt AFB, Dayton, Ohio, where it is being monitored by Dr. Rob Williams. A primary objective of this collaborative effort is to complement and augment various other ongoing research activities being conducted or supported by the Wright Labs ATR research team.

Contents

Chapter 1

Introduction and Executive Summary

As originally proposed, the primary objective of this project has been to develop algorithms for advanced air-to-ground Automatic Target Recognition (ATR) capability utilizing High Range Resolution (HRR) profiles. One of the current priority research initiatives of the Model-Based Vision Lab at USAF Wright Laboratory (WL) is to develop an advanced air-to-ground High Range resolution (HRR) Automatic Target Recognition (ATR) program. The ultimate program objective is to transition mature HRR-ATR technology into operational Air Force airborne attack and surveillance platforms. The new HRR-ATR technology will be integrated into a system approach and it is expected to vastly enhance Air Force's ability to detect, recognize, as well as identify time-critical military targets. The HRR-ATR technology would rely on processing high resolution 'Range Profiles', as distinguished from traditional SAR-ATR that utilizes SAR image data. The ATR performance with HRR is expected to be superior for Moving Targets which cause blurring in SAR data that makes recognition a difficult task. In this project, ATR algorithms based on HRR profiles are being developed initially for stationary targets for baselining purposes prior to transitioning to more critical moving targets. Research on HRR-ATR is at the stage of inception and a multifaceted approach would be essential in order to harness recent advances

from multiple disciplines.

The proposed research is being conducted in direct collaboration with Sensors Directorate's ATR Assessment Branch, Wright Laboratories, Wright-Patt AFB, Dayton, Ohio, where it is being monitored by Dr. Rob Williams. A primary objective of this collaborative effort is to complement and augment various other ongoing research activities being conducted or supported by the Wright Labs ATR group.

1.1   Status of Effort

In the past year, the major emphasis of work on this project have been devoted to three areas, as summarized below,

- **HRR Profile Data Characterization** : At the initial stage, characterization of the HRR-profile of XPATCH simulated data has been conducted including, correlation analysis, histogram analysis, Chi-square and Bispectrum-based tests of Gaussianity, Sector size analysis, Eigen analysis of HRR data, etc. The insights accumulated during the characterization study have been incorporated systematically while developing the ATR algorithms. Recently, a comprehensive measured database of Moving/Stationary Target classes (MSTAR) has also been made available, and we are currently conducting characterization studies on this new set of targets.

- **Classification using Eigen-Templates** : For this part of the project, Eigen-template based ATR is being developed as a new paradigm in ATR research. Data Characterization studies with a large class of XPATCH-simulated data indicated that the Eigen-vector corresponding to the largest Singular Value contains the majority of information about the target under consideration. Based on this crucial observation, we have focused on using the range-space eigen-vector corresponding to the largest singular value for each sector as 'Eigen-

Template' and developing a comprehensive ATR algorithm. In our work so far with eigen-templates for classification using XPATCH database (consisting of four target classes : M1 Tank, T72 Tank, School Bus and Fire Truck), we have observed significant and consistent improvement in classification performance when compared with ATR using Mean-templates. Specifically, with single observation profile for conducting ATR we have obtained greater than 99 percent classification rate for all targets classes available in the simulated XPATCH database. Currently, we are working on extending this algorithm for Measured data and Moving Targets (MSTAR). For these later target classes, some form of sequential processing using more than one observation profile may be necessary. Furthermore, the power of some targets may be distributed among more than the largest singular value and more than one eigenvector may be more appropriate for template formation.

- **Clutter Suppression using Singular Value Decomposition (SVD)** : A critical problem faced in ATR is clutter noise that corrupt the SAR images and HRR profiles. At the initial stage of this project we were conducting our baseline work using simulated XPATCH database, which is mostly clutter-free. However, we are in the process of transitioning to measured database (MSTAR) which does have clutter problem. We plan to address the clutter suppression issue using Eigen-filtering approach, which has been found to be highly successful in many other fields for noise suppression. This approach involves finding a set of orthonormal basis which best describes the subspace occupied by the signal, i.e., the signal subspace. The remaining orthogonal subspace span the clutter subspace. Our preliminary work with MSTAR data indicate that more than 90 percent energy is accounted for by less than 5 percent of singular values constituting the Signal Subspace. Hence, we do expect that eigen-filtering will

ture Radar (SAR) [6, 10, 17, 29, 40]. The original purpose for developing these radar technologies had been to achieve all-weather and all day/night imaging, *i.e.,* to transcend traditional photographic camera based imaging that must rely on sunlight and is susceptible to clouds, fog or precipitation. Both MTI and SAR are active Doppler systems that transmit and receive electromagnetic waveforms in the microwave bands that have superior penetrating capabilities than visual frequency bands. These radar technologies are being researched and developed over more than four decades now and both concepts have some share of strengths and weaknesses. MTI is a mature radar technology that allows airborne sensors to survey large areas of land and it has coarse target detection and range determination capabilities. It makes use of target movement for image formation and hence, it is highly effective for distinguishing moving targets from ground clutter. However, a major drawback of the MTI technology is its lack of any *target recognition* capability. On the other hand, SAR's ability to image ground targets with range and cross-range information gives it very good target recognition and identification capabilities, although its tremendous processing requirements prevent it from being used as a wide area surveillance technology [5, 7].

1.3 Motivation : *HRR vs. SAR*

The High Range Resolution (HRR) technology is a potential target recognition capability that promises to bridge the gap between the wide area surveillance target detection capabilities of MTI and the very narrowly focused target identification capabilities of SAR. Almost all existing SAR based ATR algorithms process detected SAR images in the azimuth (cross-range) vs. range domain, that are formed via 2-D FFT of original 'complex phase history'. Fig. 1 shows the data formation block diagram for both SAR images and HRR profiles.
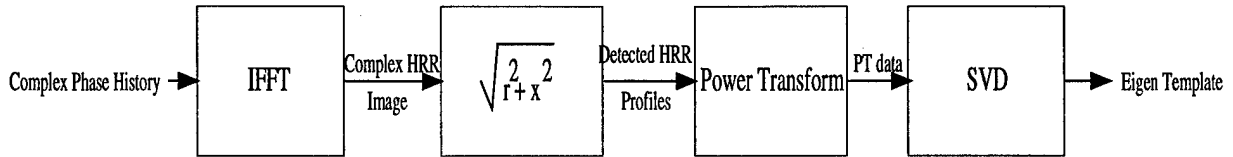
Figure 1.1: **Eigen Template Generation**

Compared to SAR-based ATR, developments using HRR data has so far been limited and is at an early stage. This is primarily because SAR-ATR's inherent capability to make use of both cross-range as well as range information, which can provide an overall depiction of the shape of a stationary target and its relative location in a scene. The range-azimuth information in SAR-images is very much analogous to 'still' photographic images and hence, SAR's usage in early ATR development is only obvious and intuitively appealing. However, it is also a common knowledge that the quality of still photography requires the objects to be in a standstill condition throughout the duration the camera lens is open. Otherwise, the quality of the developed pictures degrades due to the blurring effect caused by moving objects. This is exactly what can occur in case of SAR images when the targets to be identified are not stationary, making recognition or classification by ATR algorithms definitely a more arduous task. The primary motivation for HRR-based ATR to be undertaken in this project is to overcome this potential limitation of traditional SAR-ATR algorithms. However, for baselining purposes, stationary targets would also be considered at the preliminary stage of ATR development. Once a good understanding of stationary HRR-ATR is in place, the scope would be broadened for transitioning to Moving target ATR.

The HRR concept infuses an entirely new paradigm into SAR-ATR and its primary effectiveness and advantage are expected to be for recognition of moving targets. It may be noted that the cross-range information in SAR-images is produced by the Fourier Transform operation over a set of range profiles taken from a number of as-

pect angles. However, when a target has movement the SAR image would be blurred in the cross-range domain. Clearly, the information content of a signal or image does not change due to Fourier transformation, *i.e.*, the Range profiles contain exactly the same information on the target as does a SAR image or the complex phase history. Each individual Range profile also contains the appropriate (correct) range information for that specific angle. Hence, the key objective of the proposed research would continue to be to explore innovative ways to exploit the Range profiles directly (without the Fourier Transformation over aspect angles) in order to maximize information extraction for developing HRR-based ATR algorithms. Finally this exercise would be done by using raw MSTAR data and then the moving target data.

Journal and Conference Articles - Published/accepted/under review

- A. K. Shaw and S. Pokala, "A Structured Matrix Approach for Spatial Domain Design of 2-D IIR Filters," *IEEE Transactions on Circuits and Systems II: Analog and Digital Signal Processing*, vol. 44, no. 9, pp. 769-774, September, 1997.

- A. K. Shaw, S. Pokala R. Kumaresan, "Toeplitz and Hankel Approximation using Structured Approach," *IEEE International Conference on Acoustics, Speech and Signal Processing*, Seattle, Washington, May, 1998.

- V. Bhatnagar, A. K. Shaw and R. W. Williams, "Improved Automatic Target Recognition using Singular Value Decomposition," *IEEE International Conference on Acoustics, Speech and Signal Processing*, Seattle, Washington, May, 1998.

- A. K. Shaw, V. Bhatnagar and R. W. Williams, "ATR Using Eigen-Templates," *SPIE*, Orlando, Florida, April, 1998.

- A. K. Shaw and K. Naishadham, "Efficient ARMA Modeling of FDTD Time Sequences for Microwave Resonant Structures," *IEEE Microwave Theory and Techniques Symposium*, Denver, CO, June, 1997.

- A. K. Shaw and K. Naishadham, "Efficient Late-Time Extrapolation of FDTD Time Sequences using ARMA Modeling," *Progress in Electromagnetic Research Symposium (PIERS)*, Cambridge, MA, July, 1997.

Personnel Involved

Dr. Arnab K. Shaw (PI)

Mr. Vijay Bhatnagar (Graduate Student)

Mr. Vinay Verma (Graduate Student)

Mr. Rajesh Vashist (Graduate Student)

Chapter 2

SAR Overview

2.1   A Review of ATR

The present era of limited warfare demands precision strikes for reduced risk and cost-efficient operation with minimum possible collateral damage. In order to meet such exacting challenges, Automatic Target Recognition (ATR) capability is becoming increasingly important to the Defense community. The overall goals of ATR is to analyze image data using digital computers in order to detect, classify and recognize target signatures automatically, *i.e.*, with minimum possible human assistance. The image data for processing may be generated by one of many possible imaging sensors including radar, optical, infrared or others. ATR is considered to be one of the most challenging among current research problems because the ATR developers have little control over the possible target scenario and the operational imaging condition [1, 7, 22, 39]. Also, compared to the diversity of possible images during operations, only a relatively smaller subset of images may be available at the development or training stage. Furthermore, the operational ATR may have to deal with intelligent adversary attempting to defeat the system, as opposed to a more controlled environment during development.

Traditionally, air to ground acquisition of ground target information is categorized into two general areas: Moving Target Indication (MTI) and Synthetic Aper-

ture Radar (SAR) [6, 10, 17, 29, 40]. The original purpose for developing these radar technologies had been to achieve all-weather and all day/night imaging, *i.e.*, to transcend traditional photographic camera based imaging that must rely on sunlight and is susceptible to clouds, fog or precipitation.

2.2 Moving Target Indicator (*MTI*)

Most surface and airborne radar systems operate in an environment where the clutter return obscures targets of interest [27]. If the target is moving relative to the clutter it is possible to filter out the undesired clutter return by exploiting the differential doppler frequency shift produced by relative target to clutter radial motion. Systems following this principle are called Moving Target Indicator (MTI) radars.

MTI has the capability to detect target reflections [28] having differential radial motion with respect to the clutter. The clutter causing background may be either terrain, sea, weather or chaff [24, 35]. MTI's are operated with either fixed based or a moving platform such as an aircraft or a satellite. Considering detection of low flying aircrafts, *i.e.* the radar is surface based, flying over terrain through possible weather disturbances. In such an event, MTI rejects the returns from terrain and weather while retaining the return from the aircraft. This property gives it good detection capabilities for air borne targets. In cases where the target is surface based, as in Air to Ground ATR application, the ground clutter are stronger than the expected target return. The ground clutter extend out to a range where terrain features that cause the clutter are masked due to earth's curvature. In such cases, the ground clutter extends to the full operating range of the radar. This makes MTI without any recognition capabilities.

MTI is a mature radar technology that allows airborne sensors to survey large areas of land and it has coarse target detection and range determination capabilities.

It makes use of target movement for image formation and hence, it is highly effective for distinguishing moving targets from ground clutter. However, a major drawback of the MTI technology is its lack of any *target recognition* capability.

2.3 Synthetic Aperture Radar (*SAR*)

Although the major emphasis of this project is to utilize HRR profiles, as described in the previous chapter, it may be pointed out here that data collection as well as most of the front-end processing for HRR is identical to that of SAR. Hence, in this Section, SAR image formation is described in considerable detail.

Figure 2.1 shows the side-looking radar system wherein an aircraft carries on-board a SAR imager [17, 13] illuminates a patch of ground having a target with certain surroundings. The beam of the radar looks out to the side of the aircraft, in a direction orthogonal to its flight path. This direction of radiation propagation is referred to as the Range direction and the direction parallel to flight path is called the Cross-range direction. During the aircrafts movement, it periodically transmits pulses of microwave energy which impinge on the patch containing the target. Each of these pulses is subsequently reflected back to and received by the radar, where demodulation is performed. The assemblage of data collected and pre-processed in this manner is called a phase history and is passed on to the processor for image reconstruction. The processor could either be located on the ground or on board the flying aircraft. This processor gives out as output the electromagnetic reflectivity of the illuminated ground patch. The reflectivity is a two-dimensional function having dimensions as *Range* and *Cross-range*.

Figure 2.2 shows the SAR mechanization block diagram with digital signal processor [13]. Figure 2.6 shows the synthetic SAR images of the four XPATCH target types *viz.* M1 tank, T72 tank, School bus and Fire truck respectively. Here the magnitude

of the reflected energy can be clearly seen. Although a SAR picture looks entirely different from an optical photograph, the key features are easily recognizable. SAR is coherent radar that employs signal processing and motion compensation to provide a high spatial resolution estimate of the scenes reflectivity, also commonly known as radar cross section (RCS). Motion sensors are used to measure platform flight characteristics so that non ideal flight path generated phase errors can be removed during image formation processing. Platform or target motion creates scene aspect variations, leading to a differential doppler signature of scatterers in the antenna footprint. The doppler signatures are subsequently exploited to achieve enhanced Cross-range resolution. Doppler frequency is $1/2\pi(d\phi/dt)$, where $\phi = 4\pi R/\lambda$. This is the fundamental behind SAR imaging concept (also commonly known as Range/Doppler imaging).
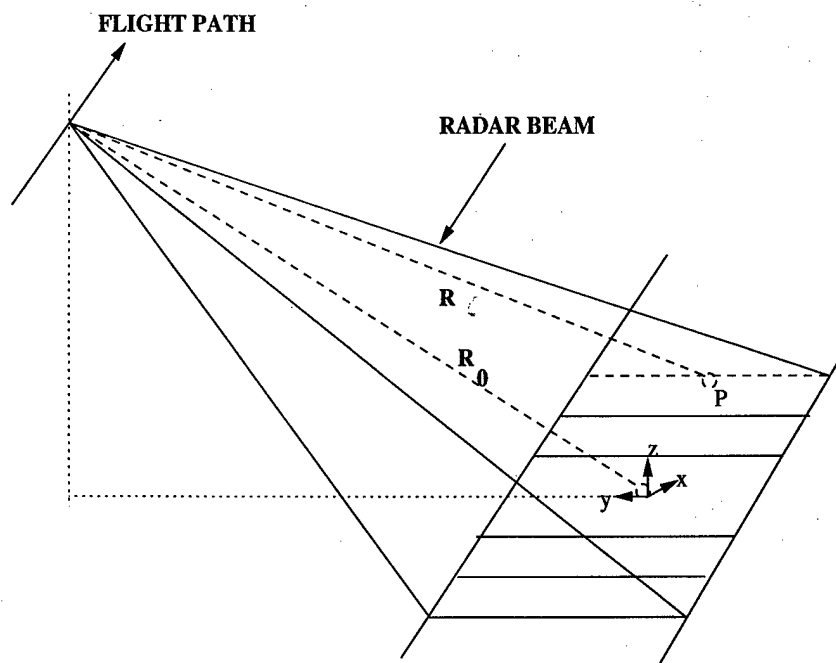
Figure 2.1: Side looking radar system geometry
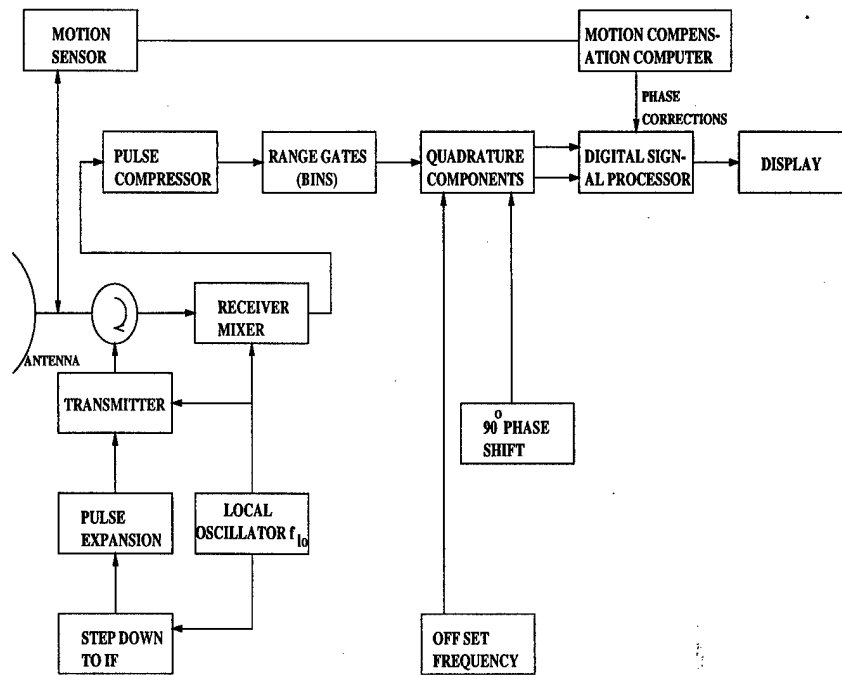
Figure 2.2: SAR Mechanization Block Diagram with Digital Signal Processor[13]

2.4   Concept of Synthetic Aperture

The fundamental behind image resolution by the concepts of image processing is the size of the antenna. In ATR applications, it is not feasible to carry huge antennas on the aircraft and therefore SAR is used. Resolution in Cross-Range can be obtained by using this concept. Considering Figure 2.5, in the previous section it is mentioned how resolution can be obtained in x-direction. As the aircraft moves, it transmits another pulse, say at an angle θ with the antenna still aiming at the center of the ground. In Figure 2.5, $(\bar{x},\bar{y})$ are the cross-range and range at angle θ, obtained by rotation of (x,y) axes. This linear transformation is orthonormal and the transformation and inverse transformation are given by [14]

$$x = \bar{x}\cos\theta - \bar{y}\sin\theta$$

$$y = \bar{x}\sin\theta + \bar{y}\cos\theta$$

$$\bar{x} = x\cos\theta + y\sin\theta$$

$$\bar{y} = -x\sin\theta + y\cos\theta \qquad (2.1)$$

Generalizing the integrated reflectivity function, $p_\theta(\bar{y})$, of two-dimensional microwave reflectivity density function, $g(x,y)$, for angle θ [14]

$$p_\theta(\bar{y}) = \int_{-L}^{L} g(x(\bar{x},\bar{y}), y(\bar{x},\bar{y}))\, d\bar{x}$$

$$= \int_{-L}^{L} g(\bar{x}\cos\theta - \bar{y}\sin\theta, \bar{x}\sin\theta + \bar{y}\cos\theta)\, d\bar{x} \qquad (2.2)$$

The return signal is given by [14]

$$r_c(t) = A_1 Re\left\{ \int_{-L}^{L} p_\theta(\bar{y}) s\left(t - \frac{2(R + \bar{y}\cos\psi)}{c}\right) d\bar{y} \right\}$$

$$= A_1 Re\left\{ \int_{-L}^{L} p_\theta(\bar{y}) \exp[j[\omega_0(t - \tau_0 - \tau(\bar{y})) + \alpha(t - \tau_0 - \tau(\bar{y}))^2]]\, d\bar{y} \right\} (2.3)$$

The return is analogous to SAR return at $\theta{=}0$ [14]

$$\bar{r}_c(t) = A_1 \int_{-L}^{L} p_\theta(\bar{y}) \exp\left[j\left[-\frac{2\bar{y}\cos\psi}{c}(\omega_0 + 2\alpha(t - \tau_0))\right]\right] d\bar{y} \qquad (2.4)$$

From equations (2.3 and 2.4), $p_\theta(\bar{y})$ can be obtained by range compression.

It can be seen that $\Delta\theta$ contains enough information to reconstruct the reflectivity density function, $g(x,y)$. From the fundamentals of SAR imagery, it can be seen that the cross-range resolution is only a function of wavelength, λ, and $\Delta\theta$. The size of $\Delta\theta$ in turn is the diversity of angles from which the pulses are transmitted and received. The standoff range of the platform are unimportant provided that the data spanning the angular interval are collected. Thus, the beneficial effects of the large antenna can be synthesized via data processing giving fine cross-range resolution independent of the operating range even with a small antenna, as in SAR. This path over which the aircraft flies is referred to as the synthetic aperture.

2.4.1 Advantages of SAR

The reasons for using SAR images over optical ones are summarized below.

- It is able to image a surface with very fine resolution of a few meters to coarse resolution of a few kilometers.

- It can provide imagery to a given resolution independently of altitude, limited only by the transmitter power available.

- A number of fundamental parameters such as polarization and look angle can be varied to optimize the system for a specific application.

- Imaging is independent of solar illumination (availability or angle) because the system provides its own source of illumination.

- It can operate independently of weather conditions if sufficiently long wavelengths are chosen.

- It operates in a band of electromagnetic spectrum different from the bands used by visible and infrared (IR) imagers.

2.5 Types of SAR:

There are primarily two types of SAR *viz.* Stripmap SAR and Spotlight SAR. Stripmap and Spotlight SAR modes are different in two ways [4]. The first difference concerns the factors that limit the azimuth resolution and and scene coverage in two modes. In Stripmap mode, Figure 2.3, antenna beam-width limits azimuth resolution and data collection length determines azimuth scene coverage. In Spotlight mode, Figure 2.4, the data collection length limits azimuth resolution and antenna beam-width determines maximum scene coverage in azimuth. The second difference involves the reference function or motion compensation signal that each mode uses

in the radar receiver. While Stripmap and Spotlight modes can transmit and receive similar signals and perform a similar range-dechirp operation, the spotlight receiver removes the azimuth chirp characteristic from all scatterers whereas the Stripmap receiver preserves it. Figure 2.3 represents a Stripmap SAR wherein the Cross Range is normal to the line of sight and apparent rotation axis of target.
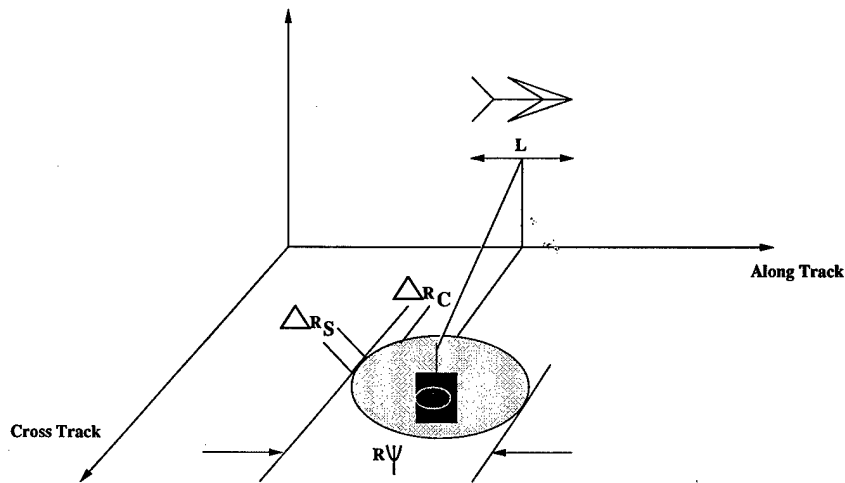
Figure 2.3: Stripmap SAR

$$\phi \;=\; \text{3dB Antenna Beamwidth} \sim \frac{\lambda}{D}$$

$$D \;=\; \text{Physical Aperture Diameter}$$

$$L \;=\; \text{VT}$$

$$T \;=\; \text{Coherent Processing Time}$$

$$V \;=\; \text{Platform Velocity}$$

The quality of stripmap SAR can be exploited by compensating for the Range difference to a Central Reference Point (*CRP*) prior to image formation. The disadvantage of stripmap SAR is the theoretical limitation in the y-resolution. Another

disadvantage is that for non-ideal flight paths, complex phase errors are created which must be removed.

Spotlight SAR [14, 41] eliminates the limitations placed on the Cross-Range resolution by the physical aperture dimension by continually tracking the *CRP*, hence allowing the integration time to be increased [41]. Based on certain observations, conclusions can be obtained. Firstly, the ability to achieve high Cross-Range resolution is limited by the migration of scatterers into neighboring resolution cells. Secondly, even a Cross-Range resolution of 1 *ft* can require large angular aperture ($\sim 10°$), resulting in significant blurring due to scatterer migration. This becomes evident at low frequencies since a large coherent processing angle is required for a given Cross-Range resolution ($\Delta R = \frac{\lambda}{2\delta\phi}$). Thirdly, the image blurring becomes significant as the migration of scatterers approaches the desired resolution. All these factors make recognition hard for moving targets. In case of HRR profiles, all the information in range is still present, but the cross-range blurring is not present.
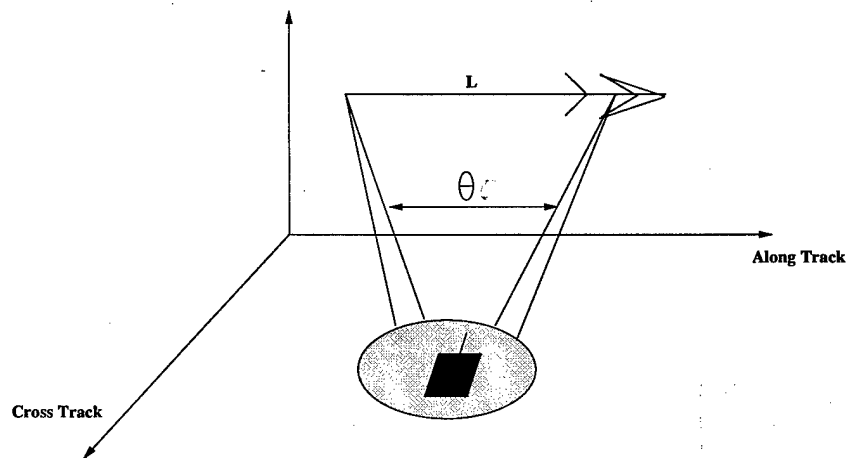
Figure 2.4: Spotlight SAR
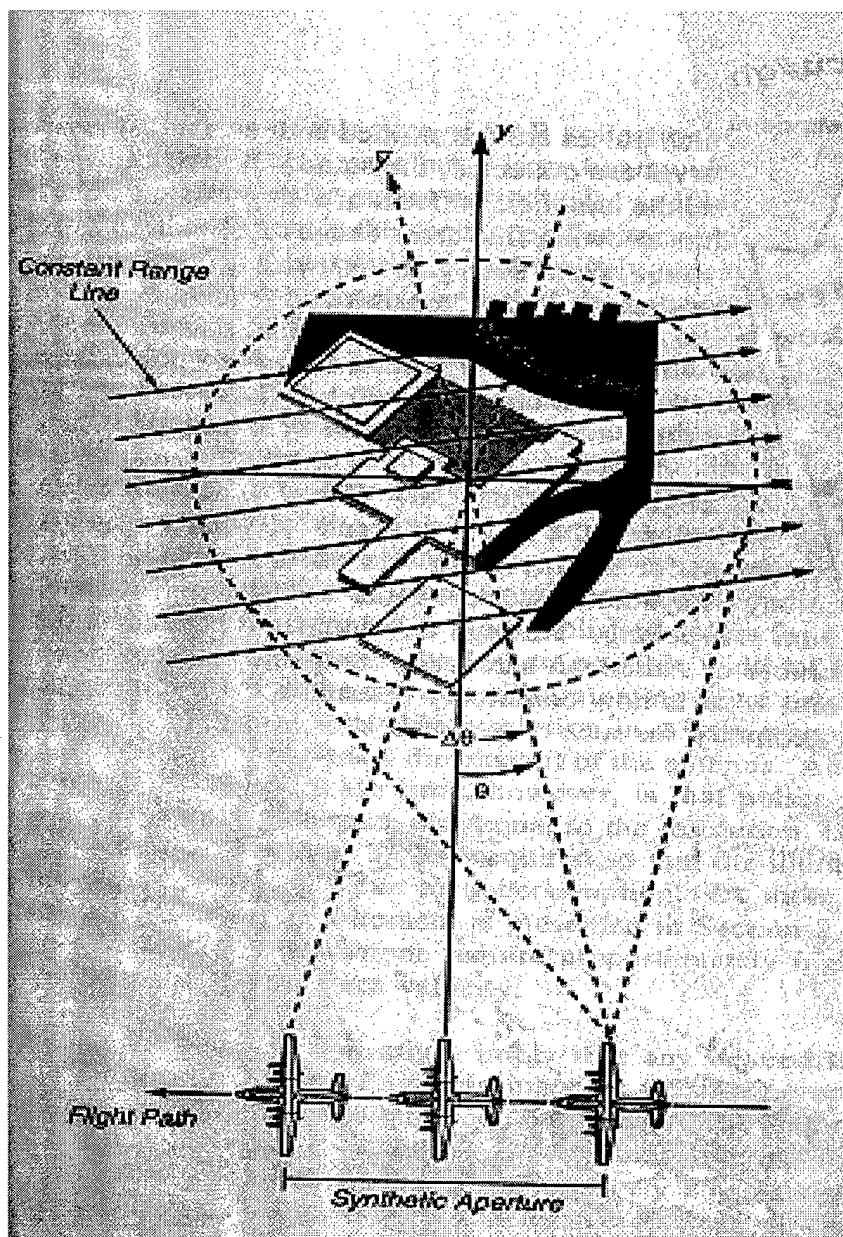
Figure 2.5: Concept of Synthetic Aperture [14]

Chapter 3

HRR data generation and Preprocessing

The HRR-ATR technology relies on processing high resolution 'Range Profiles', as distinguished from traditional SAR-ATR that utilizes SAR image data. The ATR performance with HRR is superior for Moving Targets which cause blurring in SAR data that makes recognition a difficult task.

Currently, Automatic Target Recognition (ATR) is performed primarily using Synthetic Aperture Radar (SAR) [20, 21] images. ATR using SAR images performs poorly in case of moving targets due to blurring caused in the cross-range domain, as discussed in previous Chapters. Moreover, there are considerable savings in front-end processing in producing HRR profiles which require only 1-D FFT operation, as opposed to SAR's use of 2-D FFT (see 3.2). The processing factor becomes significant in case of on-line processing because in order to produce a single SAR image, radar returns must be generated over a relatively large sector angles (2 to 2.5 degrees). With HRR profiles, only a relatively small number of angles would be sufficient to perform ATR. Figure 3.2 shows the process of generating HRR profiles from Complex Phase History (CPH). As shown in the figure, SAR image can be obtained from the HRR profiles by taking Fourier transform in the angle-domain to produce the cross-range information.

The Range Swath to be imaged is defined a-priori based on Altitude and depression angle of radar. This makes a fixed sampling window. The two primary HRR waveforms for SAR systems are the Frequency stepped and Linear Frequency modulation. The Range resolution (ΔR) is determined by the radar RF bandwidth. Thus, the resultant received signal ($Y(\tau_j)$) in each Range gate would be [41]

$$Y(\tau_j) \propto \left| \sum_{i=1}^{N} \sqrt{\sigma_i} e^{\frac{j4\pi R_i}{\lambda}} \right|^2$$

where σ_i is the *RCS* of elemental scatterers in Range gate, R_i is the Range to scatter and N is the number of scatterers in a Range gate.

The chapter is organized as follows

First, the optimum sector size is determined based on correlation analysis. Then the effect of Power-transform coefficient, in pre-processing stage, on the ATR efficiency is explored. Finally, it is shown that Normalization after Power-transform improves ATR results (Figure 4.17). The effect of changing sequence of different pre-processing operations on ATR performance is also discussed.

3.1   HRR Profile Data Characterization

3.1.1   Correlation analysis and Sector size determination

Prior to developing an ATR algorithm, a decision must be made regarding how the Template or Feature set Library should be formed using the Training data set. This is an important computational trade-off issue. If large number of independent templates are formed using relatively short training data sectors, Classification performance should be enhanced. However, a possible drawback of this approach is that the on-line ATR decision process would be more time intensive. On the other hand, if template library is made too short to achieve fast ATR decision, classification performance may deteriorate. For the synthetic XPATCH database a compromise was reached
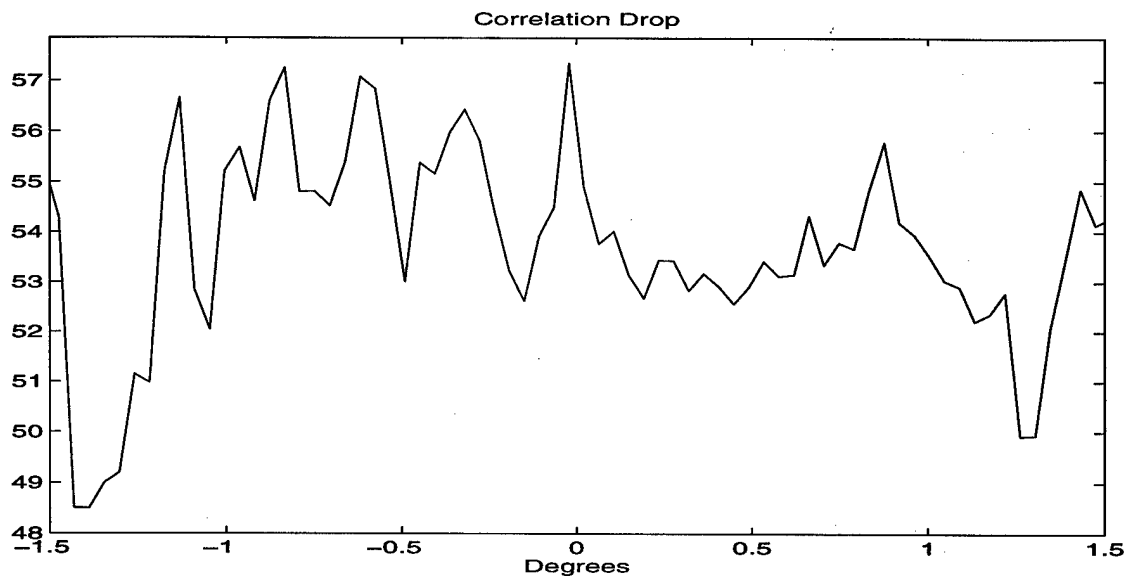
Figure 3.1: Correlation Drop for the 59th look for M1 tank in 120° − 125° sector within 3° looks

based on correlation analysis. The correlation study, as in Figure 3.1, indicated that data-correlation drops significantly after about 2.5° in correlation lag, 1.25° on each side in figure 3.1. This analysis matches spot-light made collection of training data simulated by XPATCH. Hence, in our ATR algorithms training templates were formed with each 2.5° non-overlapping sectors. If the sector size is decreased from figure 3.1, the number of sectors would increase, which will increase the computation time. On the other hand, if the sector size is increased, due to lack in correlation, the ATR performance would be affected.

3.1.2 Creation of HRR profiles

Once the decision on the sector size has been taken and the Complex Phase History (CPH) is broken down into these sectors, the next step involves obtaining the HRR profiles for each sector. Figure 3.2 depicts the process of generating detected HRR profiles (Range *vs.* Angle) and SAR image (Range *vs.* Cross-range) from raw Complex Phase History (Frequency *vs.* Angle). Figure 3.5 shows the power-transformed HRR

profiles of the four targets, *M1, T72, FT* and *SB*.
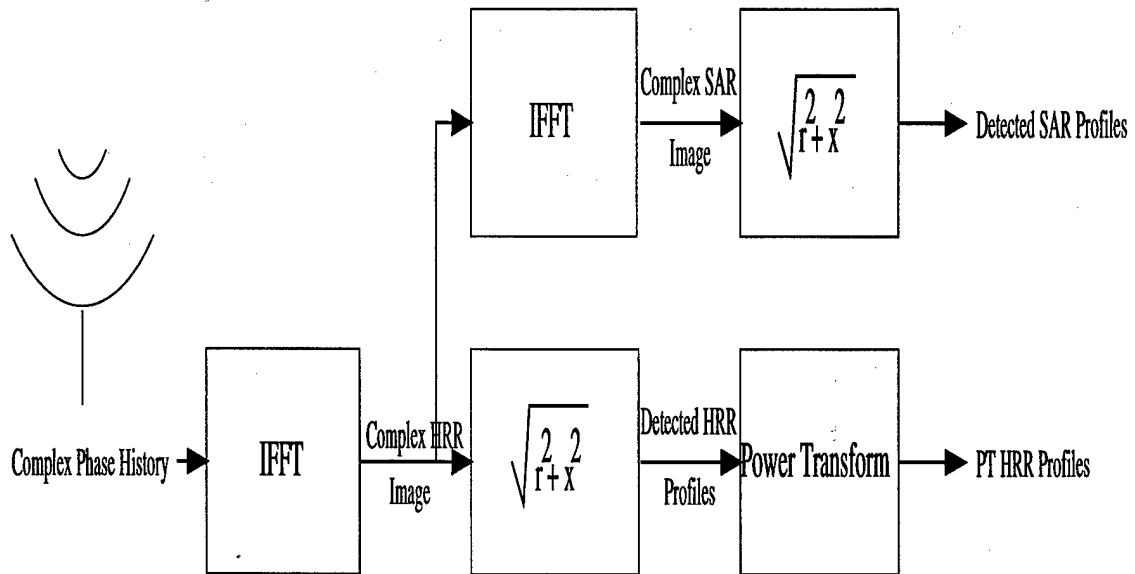
Figure 3.2: HRR and SAR Profile Generation

3.1.3 Power Transform operation

HRR-data used in this project for developing ATR algorithms is known as the Detected-HRR because it is formed using the absolute value of the Complex HRR data obtained via 1-D FFT of Complex Phase History. Detected HRR is positive valued and tend to be Rayleigh distributed for which optimum detection/estimation results are not straight-forward. Gaussian Distribution, on the other hand, can have clear advantage because many commonly used detection/estimation algorithms can be shown to possess optimality properties for the Gaussian case. In Pattern Recognition context, Fukunaga [9] has shown that it is advantageous to convert the distribution to a normal-like one by using a transformation such as:

$$Y = X^v \qquad (0 < v < 1) \qquad (3.1)$$

According to Fukunaga, the input distribution of input X, gets converted to a normal distribution of output Y. Let M be the Expected vector and $\sum$ the covariance

matrix of X. Then, the normalized distance of X from M is given by [9] distribution of X with the matrix $\sum$, the normalized [9]

$$d^2 = (X-M)^T {\sum}^{-1} (X-M) = Z^T Z = \sum_{i=1}^{n} z_i^2 \qquad (3.2)$$

where $Z = A^T(X-M)$ and A is whitening transformation. Since the expected vector and covariance matrix of Z are 0 and I respectively, z_i's are uncorrelated, $E\{z_i\}=0$ and $Var\{z_i\}=1$. The expected value and variance of d^2 are

$$E\{d^2\} = nE\{z_i^2\} = n \qquad (3.3)$$

$$
\begin{aligned}
Var\{d^2\} &= E\{(d^2)^2\} - E^2\{d^2\} \\
&= \sum_{i=1}^{n} E\{z_i^4\} + \sum_{i=1}^{n}\sum_{\substack{j=1 \\ i \neq j}}^{n} E\{z_i^2 z_j^2\} - n^2 E^2\{z_i^2\} \qquad (3.4)
\end{aligned}
$$

If z_i^2's are uncorrelated, $i.e$ z_i's are independent, and $E\{z_i^4\}$ is independent of i, the variance can be simplified to

$$Var\{d^2\} = n\gamma \qquad (3.5)$$

The γ for such a function, in equation (3.5) can be written as

$$\gamma = E\{z_i^4\} - E\{z_i^2\} = E\{z_i^4\} - 1 \qquad (3.6)$$

A gamma density function is of the form [23]

$$f(k) = Gk^\beta e^{-\alpha_i k} u(k) \qquad (3.7)$$

where u is the unit step function. In equation (3.7), numbers β and α_i are positive and G can be obtained from

$$\int_0^\infty G k^\beta e^{-\alpha_i k} \, dk = 1 \qquad (3.8)$$

Solving equation (3.8), we get

$$G = \frac{\alpha_i^{\beta+1}}{\Gamma(\beta+1)} \qquad (3.9)$$

$$\text{where} \qquad \Gamma(\beta) = \int_0^\infty l^{\beta-1} e^{-l} \, dl \qquad (3.10)$$

It is known that the sample variance $\hat{c}_{ii} = 1/(N-1) \sum_{k=1}^N (x_{ik} - \hat{m}_i)^2$ for a normal x_i has a gamma distribution. The gamma distribution for $\hat{c}_{ii}$ can be obtained by equation (3.7) as

$$f_{\hat{c}_{ii}}(k) = \frac{\alpha_i^{\beta+1}}{\Gamma(\beta+1)} k^\beta e^{-\alpha_i k} u(k) \qquad (3.11)$$

where

$$\beta + 1 = \frac{N-1}{2} \qquad (3.12)$$

$$\alpha_i = \frac{N-1}{2\sigma_i} \qquad (3.13)$$

and Γ, from equation (3.10), is the gamma function. In equations (3.3) and (3.5), only the first two moments of d^2 are shown. However, if z_i's are normal, the density function of d^2 would again be gamma density and can be obtained by using equation (3.7) as

$$f_{d^2}(\varrho) = \frac{1}{2^{n/2} \Gamma(n/2)} \varrho^{\frac{n-2}{2}} e^{-\varrho/2} u(\varrho) \qquad (3.14)$$

In equation (3.14), $\beta = n/2 - 1$ and $\alpha = 1/2$. For equation (3.14), $E\{d^2\} = \frac{\beta+1}{\alpha} = n$ and $Var\{d^2\} = \frac{\beta+1}{\alpha^2} = 2n$. These values when compared with equations (3.3) and (3.5),

give $\gamma=2$. Since Z is a linear transformation on X, Z is normal given X is normal for this value.

Y of equation (3.1) will be normal by making γ of equation (3.5) close to 2. Here, $\gamma_y = E\{(y-\bar{y})^4\} - E^2\{(y-\bar{y})^2\} \approx 2$, under the condition $E\{(y-\bar{y})^2\}=1$, where $\bar{y}=E\{y\}$. X in equation (3.1) has a gamma density function as shown in equations (3.7) and (3.11). Based on this, the moments of Y would be

$$
\begin{aligned}
E\{y^m\} &= \frac{\alpha^{\beta+1}}{\Gamma(\beta+1)} \int_0^\infty x^{vm} x^\beta e^{-\alpha x}\, dx \\
&= \frac{1}{\alpha^{mv}} \frac{\Gamma(\beta+1+mv)}{\Gamma(\beta+1)}
\end{aligned}
\tag{3.15}
$$

Finding γ_y, we get

$$
\begin{aligned}
\gamma_y &= \frac{E\{(y-\bar{y})^4\} - E^2\{(y-\bar{y})^2\}}{E^2\{(y-\bar{y})^2\}} \\
&= \frac{E\{y^4\} - 4E\{y^3\}E\{y\} + 6E\{y^2\}E^2\{y\} - 3E^4\{y\}}{[E\{y^2\} - E^2\{y\}]^2}
\end{aligned}
\tag{3.16}
$$

Using (3.15) in (3.16), γ_y turns out to be a function of β and v only as α's of numerator and denominator cancel out. It is realized, from figure 3.3 that for a particular fixed value of v, γ_y can be fixed for a wide range of β. As we lower v, irrespective of value of β, the γ_y settles around 2, which is the requirement for normality. The class separability, in turn recognition, can be done more easily by doing this transformation as Y in (3.1) is normal. The design of the classifier also becomes easier, because a standard quadratic classifier could be used rather than a designing a complicated classifier, as shown in Figure 4.16. The important property of this transformation is that the correlation coefficients are more or less unaffected as shown next. The Taylor series expansion of equation (3.1) gives [9]
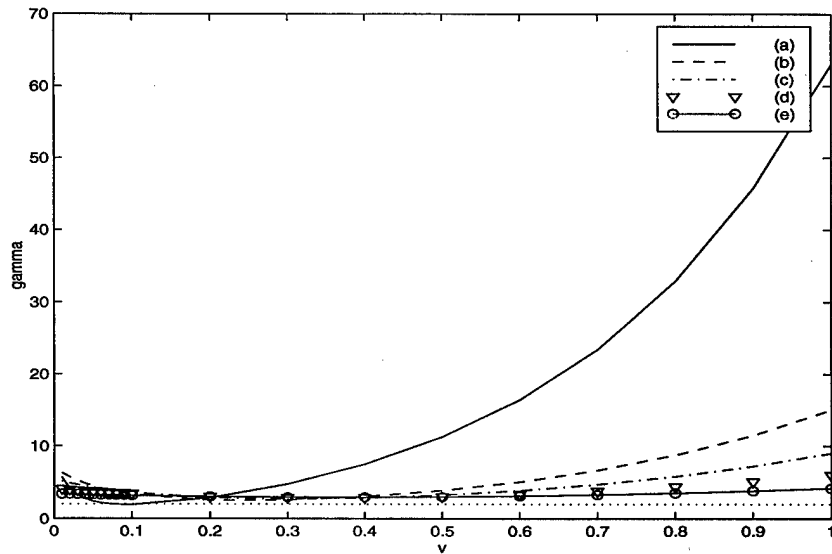
Figure 3.3: Variation of γ with v for; (a) $\beta = -0.9$ (b) $\beta = -0.5$ (c) $\beta = 0$ (d) $\beta = 1$ (e) $\beta = 4$ [9]

$$y_i \cong \mu_{x_i}^v + v\mu_{x_i}^{v-1}(x_i - \mu_{x_i}) \tag{3.17}$$

$$\mu_{y_i} \cong \mu_{x_i}^v \tag{3.18}$$

$$\sigma_{y_i}^2 \cong (v\mu_{x_i}^{v-1})^2\sigma_{x_i}^2$$

$$\rho_{y_iy_j} \cong \frac{E\{(y_i - \mu_{x_i}^v)(y_j - \mu_{x_j}^v)\}}{\sqrt{\sigma_{y_i}^2\sigma_{y_j}^2}}$$

$$\cong \frac{(v\mu_{x_i}^{v-1})(v\mu_{x_j}^{v-1})E\{(x_i - \mu_{x_i})(x_j - \mu_{x_j})\}}{\sqrt{(v\mu_{x_i}^{v-1})^2\sigma_{x_i}^2(v\mu_{x_j}^{v-1})^2\sigma_{x_j}^2}}$$

$$= \rho_{x_ix_j} \tag{3.19}$$

The result is valid for all first order approximations, as our case. The lower the value of v the better is the chance to design a good linear classifier. This comes from two facts. Firstly, considering equation (3.17), in an exponential distribution, $\beta=0$ and $E^2\{x\} = Var\{x\}$, the second order approximation of equation (3.18) becomes

$$\mu_y \cong \mu_x^v + \frac{v(1-v)}{2}\mu_x^{v-2}E\{(x - \mu_x)^2\}$$

$$= \left[1 + \frac{v(1-v)}{2} \right] \mu_x^v \qquad (3.20)$$

If (3.20) is calculated for lowering v, then (3.20) tends more to (3.18), as desired in a first order approximation. Secondly, in general, for normal distributions, for a two vector case, the Bhattacharya distance is given by [2]

$$\mathcal{B}(1/2) = \frac{1}{8}(M_2 - M_1)^T \left[\frac{\Sigma_1 + \Sigma_2}{2} \right]^{-1} (M_2 - M_1) + \frac{1}{2} \ln \frac{\left| \frac{\Sigma_1 + \Sigma_2}{2} \right|}{\sqrt{|\Sigma_1||\Sigma_2|}} \qquad (3.21)$$

The term $\mathcal{B}(1/2)$ is called the Bhattacharya distance. It is the optimum solution to the popularly known Chernoff bound for calculation of upper bounds in Bayes error. In (3.21), the first term represents the class separability due to their mean-difference while the second term gives the class separability due to covariance difference. It comes to light that the weight of first term of the Bhattacharya distance dominates as we further lower v. The theory was realized in table was lowered from 0.4 to 0.08, more number of vectors passed the Pearsons chi-square test for normality.

3.1.4 Effect of Template and Observation data Normalization

In case of HRR profiles, the crucial information on the differences between various target classes are contained in the respective range profile structures. The relative amplitudes in the range profiles depend on the strengths of the radar returns from the scattering centers and the relative positions of the scattering centers of a particular target. However, the total template energy of one target may be significantly stronger than other classes, due to amplification or attenuation during data collection. In that case, the signal strength (or energy) and not the relative variations in range profile structures may dominate and overwhelm the ATR decision process. Figure 3.4 depicts a possible scenario where un-normalized templates for four target classes are

represented by the blobs. The lines connecting the centroids of the blobs to origin represent the energy whereas the blobs themselves and the angles made with the axes signify the variations in scattering returns for different targets. For this assumed but typical scenario, T72 appears to dominate due to its total signal energy whereas the School Bus profile has the least energy. If ATR decision is made by correlating these templates with an observed range profile to look for a maxima (*i.e.* Match Filtering), T72 will tend to dominate regardless of the actual target producing the observation profile.

<div align="center">(a)</div>
<div align="center">(b)</div>
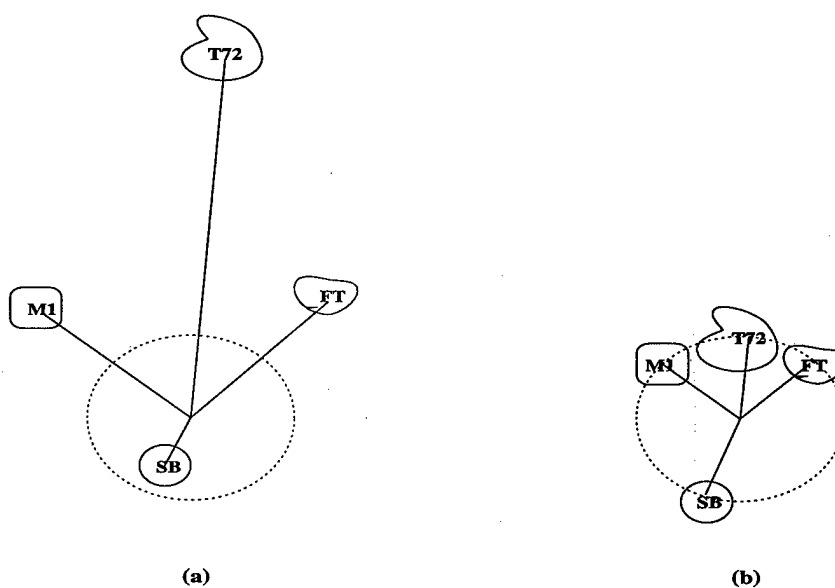
Figure 3.4: Effect of Normalization on target recognition, (a) before Normalization (b) after Normalization

The scaling problem depicted in Figure 3.4(a) is usually resolved using some form of least-squares (LS) algorithm using a linear model [42]. However, the linear model assumption appears to be ad hoc and is not necessarily unique, depending possibly on data type which in turn may affect classification performance. Instead, it is proposed to use normalized templates, as depicted by Figure 3.4(b), where the template profiles for all targets are normalized to have same length (*i.e.*, energy), while preserving their angular separations and relative variations in scattering returns as represented

by the blobs. If an observed profile is to be compared with these templates to make an ATR decision, then simple matched filtering (MF) will be sufficient for the purpose. It may be noted here that normalization of templates can be performed off-line and furthermore, MF requires less on-line processing than LS because no matrix inversion is necessary. It is observed (Figure 4.17) that this technique works very well if recognition is done by matched filtering. Extensive simulation performed for this thesis indicate that both power-transform operation followed by the data normalization yield the best overall classification performance (Figure 4.16).
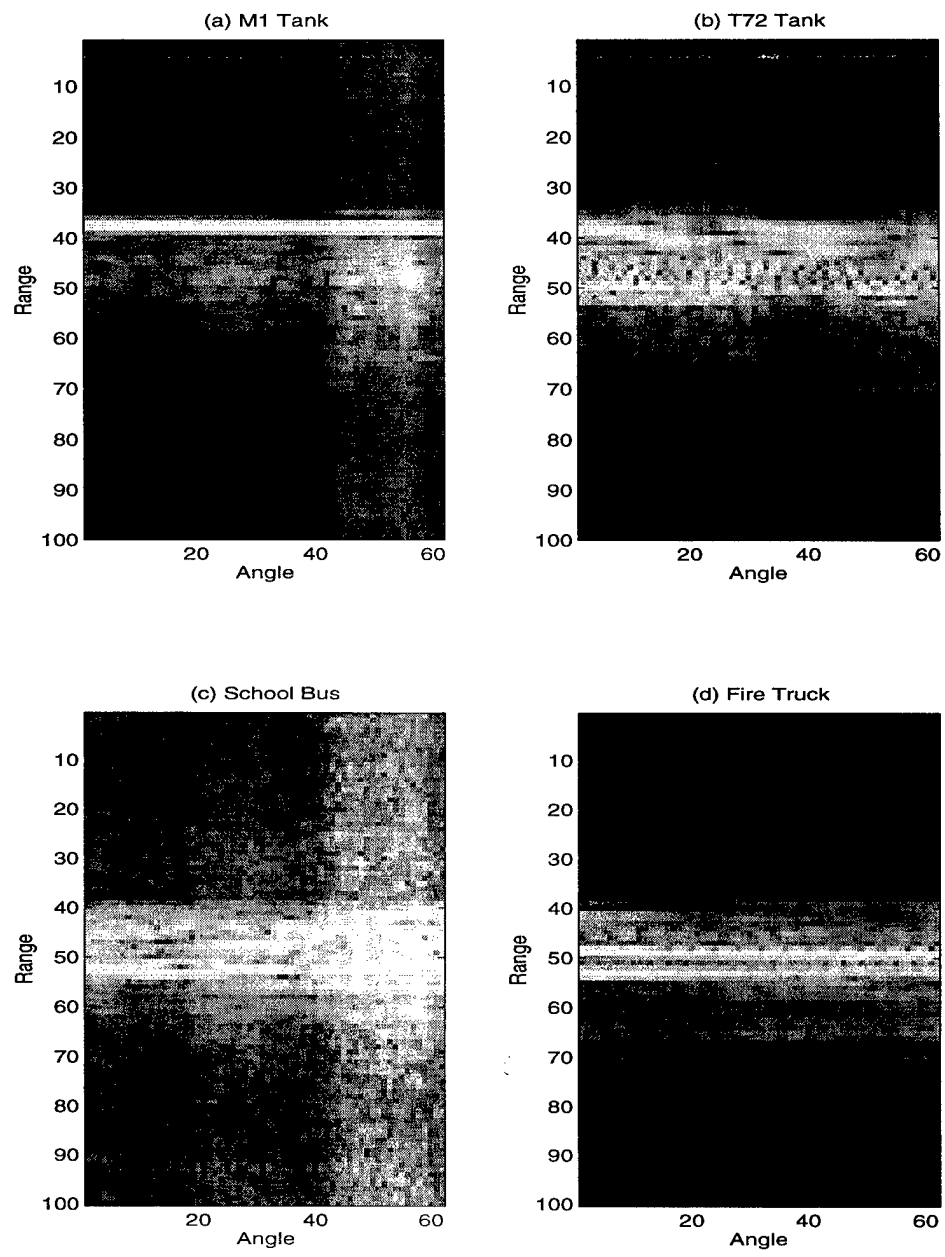
Figure 3.5: Power transformed HRR profiles for (a) M1 Tank (b) T72 Tank (c) School Bus (d) Fire Truck, 60-62.5° template, v = 0.08

Chapter 4

Feature Extraction, Clutter Suppression and Classification

The goal of feature extraction is to transform from a n-dimensional feature space to a smaller m-dimensional feature space such that most of the information is retained after the mapping. The axis which defines this new co-ordinate space, m, is called the feature space [36, 37]. The primary advantage of doing this "mapping transformation" is to reduce the dimensional space of the data, in turn decreasing computation. This procedure also reduces clutter effects, which can give highly misleading results at the recognition stage. Optimal feature set can be interpreted as a set in which if any further feature is added, the information content does not increase. Optimal feature set can also be defined as a set of features which do not increase the minimum probability of error in all events. The HRR profiles usually have clutter in them and in this chapter a new approach has been proposed for extracting best features that also has the inherent capability to suppress clutter at the same time. The probability of error is minimized to obtain this optimal feature set.

The previous approach for feature extraction is mean-based [42]. This approach works well other than the cases where the mean vector of the classes come near to each other or the variance becomes large. A new approach using the technique of Eigen-analysis is used to obtain the feature set. This technique gives classification

rates as high as 99.5%.

4.1 Mean-Based Feature Extraction

The mean-based approach for HRR Template formation is via averaging of the range profiles over a section of contiguous aspect angles and these are called Mean-Templates [42]. Let $\mathbf{Y} \stackrel{\triangle}{=} [\mathbf{y}_1 \ \mathbf{y}_2 \ \ldots \ \mathbf{y}_M]^T$ be an $N \times M$ matrix containing power transformed range profiles of the "Training" data set, at M angular looks containing N range gates each. The mean template can be formed as,

$$\mathbf{t} \stackrel{\triangle}{=} \frac{1}{M} \sum_{i=1}^{M} \mathbf{y}_i \tag{4.1}$$

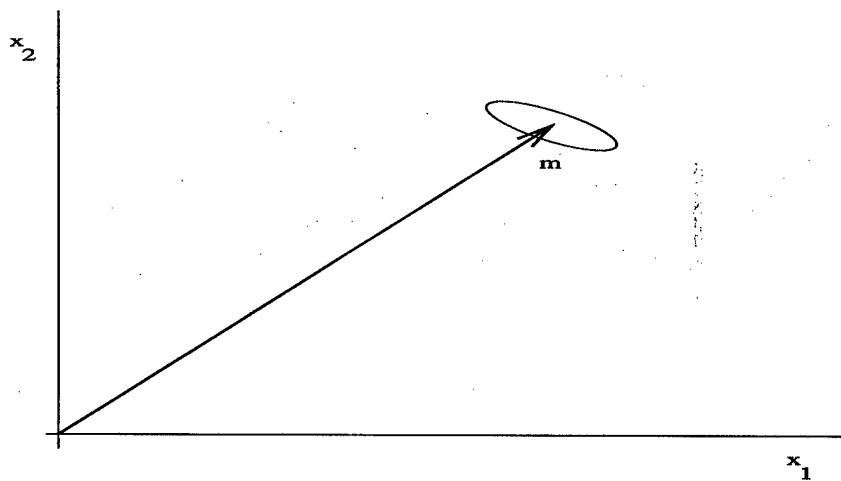Figure 4.1: A typical case where mean-based classifier performs well [37]

If the mean vector is large compared to the variances, as in Figures 4.1 and 4.2 then according to [37], the optimal features chosen will be in the general direction of the mean-vector. The correlation matrix, in such an event, is strongly influenced by the mean as shown in equation (4.2). The covariance matrix, $\mathbf{K}$, can be written as [37]
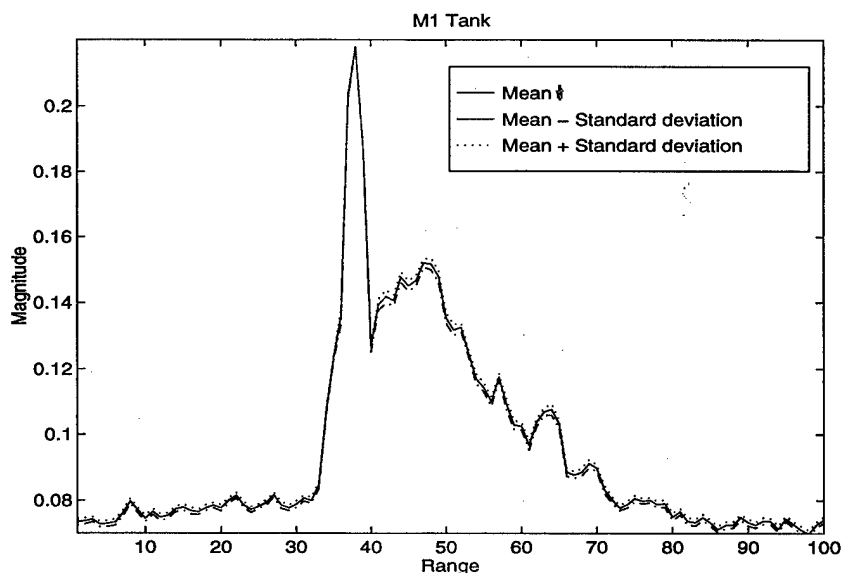
Figure 4.2: Variation of Range profile formed using mean-based approach with the Standard deviation for M1 Tank, $60° - 62.5°$ sector, $v{=}0.08$

$$\mathbf{K} \;\triangleq\; E\{(\mathbf{y} - \mu)(\mathbf{y} - \mu)^T\} = E\{\mathbf{y}\mathbf{y}^T - \mathbf{y}\mu^T - \mu\mathbf{y}^T + \mu\mu^T\}$$

$$= \; E\{\mathbf{y}\mathbf{y}^T\} - \mu\mu^T \tag{4.2}$$

In equation (4.2), $E\{yy^T\}$ is the correlation, given by $\mathbf{R}$. Equation (4.2) follows to

$$\mathbf{R} = \mathbf{K} + \mu\mu^T \tag{4.3}$$

4.2 Eigen-Template Features from Singular Value Decomposition (SVD)

Singular Value Decomposition (SVD) is a very effective and robust tool for decomposing any matrix into orthogonal basis spaces. SVD analysis of HRR data revealed significant underlying properties about the target classes under consideration. SVD projects the information content of a matrix onto its orthogonal basis spaces. Let
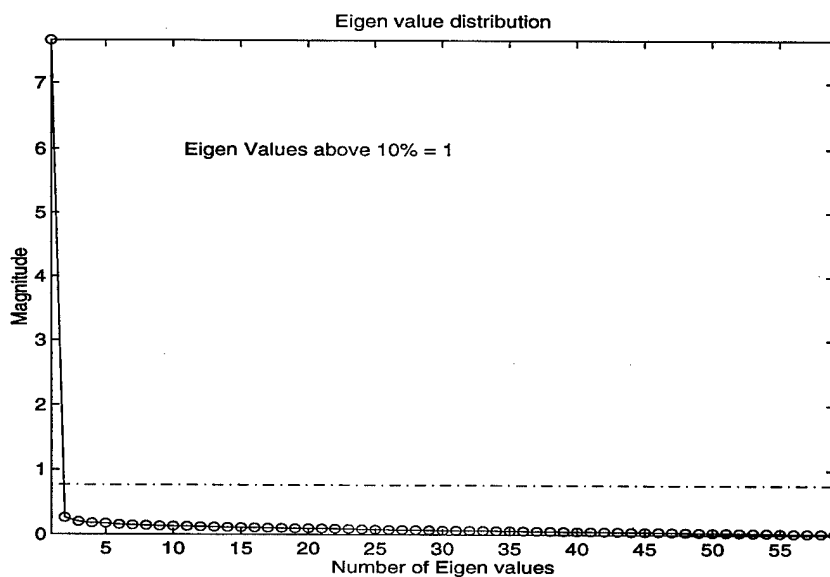
Figure 4.3: Distribution of Singular values for XPATCH target $T72$, $60° - 62.5°$ sector, $v=0.08$

$\mathbf{Y}$ be an $N \times M$ matrix containing power transformed range profiles at M angular looks containing N range gates each. The SVD operation would produce a basis decomposition into three matrices,

$$\mathbf{Y} \stackrel{\text{SVD}}{\Longrightarrow} \mathbf{U}\Lambda\mathbf{V}^T \tag{4.4}$$

where,

$$\begin{aligned}
\mathbf{U} &\triangleq \text{EV}[\mathbf{Y}\mathbf{Y}^T] \\
&= \begin{bmatrix} u_{11} & \cdots & u_{1N} \\ \vdots & \ddots & \vdots \\ u_{N1} & \cdots & u_{NN} \end{bmatrix} \\
&= \begin{bmatrix} \mathbf{u}_1 & \mathbf{u}_2 & \cdots & \mathbf{u}_N \end{bmatrix} \in \text{IR}^{N \times N}
\end{aligned} \tag{4.5}$$

$$\Lambda = \begin{bmatrix} \lambda_{11} & & & \mathbf{0} \\ & \lambda_{22} & & \\ & & \ddots & \\ & & & \lambda_{MM} \\ \mathbf{0} & & & 0 \end{bmatrix} \in \text{IR}^{N \times M} \tag{4.6}$$

Figure 4.4: A Typical Eigen template for XPATCH target $T72$, $60° - 62.5°$ sector, $v=0.08$

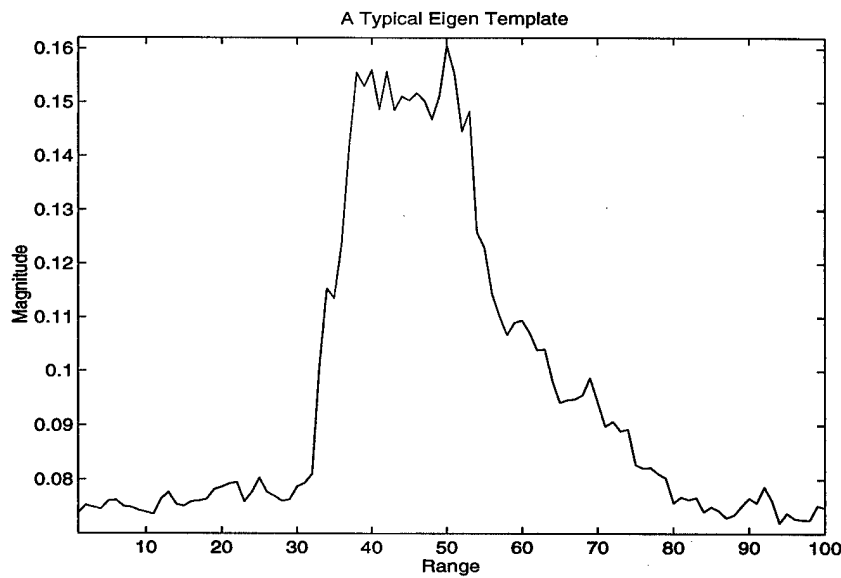$$\mathbf{V} \triangleq \text{EV}[\mathbf{Y}^T\mathbf{Y}]$$

$$= \begin{bmatrix} v_{11} & \cdots & v_{1M} \\ \vdots & \ddots & \vdots \\ u_{M1} & \cdots & u_{MM} \end{bmatrix}$$

$$= \begin{bmatrix} \mathbf{v}_1 & \mathbf{v}_2 & \cdots & \mathbf{v}_M \end{bmatrix} \in \mathbf{IR}^{M \times M} \qquad (4.7)$$

where, EV[·] denotes the operation "Eigenvectors of". For Range *vs.* Angle HRR data, the left eigenvectors in $\mathbf{U}$ span the orthogonal basis space in the range domain while the right eigenvectors in $\mathbf{V}$ span the angle space. Λ is a diagonal matrix containing M (or N, depending on which is larger. $N > M$ is assumed here implicitly) singular values in decreasing order, *i.e.* $\lambda_{11} \geq \lambda_{22} \geq \cdots \geq \lambda_{MM}$, with λ_{ii} representing the weights associated with the i-th eigenvector. Larger singular values imply significant contribution of that particular eigenvector in forming the target signal. Hence those are denoted as "signal subspace" eigenvectors. Interestingly, the range-space in $\mathbf{U}$ and angle-space eigenvectors in $\mathbf{V}$ appear in *decoupled* form after the SVD transformation is applied to $\mathbf{Y}$, as shown in (4.4).

The primary focus of this project so far has been to exploit the information contained in the decoupled range basis space vectors in $\mathbf{U}$ to perform ATR. The basis spaces associated with the larger singular values correspond to the underlying signal-subspace, whereas those corresponding to the smaller singular values correspond to the "noise or Clutter subspace" [30]. In order to suppress noise, one simply uses the projection of the received signal onto the signal subspace in a process known as Eigen-Filtering. In particular, only 1 out of more than 100 singular values were found to account for more than 90% of energy. Figure 4.3 illustrates this fact where the singular values for the XPATCH data type is shown. As observed, only 1 Eigen value (λ_{11}) makes up more than 90% of the total energy of the distribution. It was also noted that the left eigenvector $(\mathbf{u}_1)$ corresponding to the largest singular value (λ_{11}) possessed all the characteristics of a range profile (because it is the maximized projection). This approach of utilizing range-space eigenvectors as templates appears to be new in HRR-ATR.

4.2.1 Optimal Feature Selection [37]

In this section it is demonstrated that the eigenvectors corresponding to the larger eigenvalues of correlation matrix constitute the optimum feature set in the mean-squared error sense. Consider finding features for a random vector $\mathbf{y}$ of dimension n by a linear combination of $m < n$ vectors from some orthonormal basis, $\mathbf{u}_1$, $\mathbf{u}_2$, ..., $\mathbf{u}_m$, *i.e.*,

$$\hat{\mathbf{y}} = f_1\mathbf{u}_1 + f_2\mathbf{u}_2 + \cdots + f_m\mathbf{u}_m$$

$$= \mathbf{U}_m f \quad \text{where,} \tag{4.8}$$

$$f_j = \mathbf{u}_j^T \mathbf{y} \tag{4.9}$$

are the coefficient to be optimized by minimizing the Mean-Squared Error (MSE). Since $\mathbf{u}_j$ is an orthonormal basis, the residual error is [37]

$$
\begin{aligned}
\epsilon &= \mathbf{y} - \hat{\mathbf{y}} \\
&= \sum_{j=m+1}^{n} f_j \mathbf{u}_j
\end{aligned}
$$
(4.10)

In order to minimize MSE

$$
\begin{aligned}
\xi &= E[|\mathbf{y} - \hat{\mathbf{y}}|^2] \\
&= E[\epsilon^T \epsilon] \\
&= E\left[\left(\sum_{i=m+1}^{n} f_i \mathbf{u}_i^T\right)\left(\sum_{j=m+1}^{n} f_j \mathbf{u}_j\right)\right] = \sum_{j=m+1}^{n} E[f_j^2]
\end{aligned}
$$
(4.11)

(4.12)

where using (4.9)

$$
f_j^2 = (\mathbf{u}_j^T \mathbf{y})(\mathbf{y}^T \mathbf{u}_j)
$$

Thus, $\quad E[f_j^2] = \mathbf{u}_j^T E[\mathbf{y}\mathbf{y}^T]\mathbf{u}_j = \mathbf{u}_j^T \mathbf{R} \mathbf{u}_j$
(4.13)

where $\mathbf{R}$ is the correlation matrix of $\mathbf{y}$. Using equation (4.13) in (4.12),

$$
\xi = \sum_{j=m+1}^{n} \mathbf{u}_j^T \mathbf{R} \mathbf{u}_j
$$
(4.14)

Equation (4.14) is met under the constraint that

$$
\mathbf{u}_j^T \mathbf{u}_j = 1 \qquad j = m+1, \cdots, n
$$
(4.15)

The above problem, minimizing (4.14) under the constraint of (4.15), can be solved using Lagrange multipliers λ_j and minimizing,

$$\xi' = \sum_{j=m+1}^{n} \mathbf{u}_j^T \mathbf{R} \mathbf{u}_j + \sum_{j=m+1}^{n} \lambda_j (1 - \mathbf{u}_j^T \mathbf{u}_j) \tag{4.16}$$

The condition for the minimum in equation (4.16) becomes

$$\frac{\partial \xi'}{\partial \mathbf{u}_j} = 2(\mathbf{R} \mathbf{u}_j - \lambda_i \mathbf{u}_j) = 0, \qquad j = m+1, \cdots, n \tag{4.17}$$

From equation (4.17), $\mathbf{u}_j$ must be the Eigen vectors of $\mathbf{R}$. Under this condition and using equation (??), equation (4.14) reduces to [12]

$$\xi = \sum_{j=m+1}^{n} \lambda_j \tag{4.18}$$

Thus, the eigen vectors corresponding to the m largest Eigen values constitute the "optimal feature set" in the minimum mean squared error sense.

It may be noted here that when dealing with measured range profile data available for training, the correlation matrix $\mathbf{R}$ has to be estimated because it is impossible to know the theoretical $\mathbf{R}$. If matrix $\mathbf{Y}$ contains the training profiles, the range-space correlation matrix can be estimated as,

$$\mathbf{R} \triangleq \mathbf{Y} \mathbf{Y}^T. \tag{4.19}$$

It may be recalled from (4.4)-(4.5) that the left eigen-vectors ($\mathbf{U}$) produced by SVD are the eigen-vectors of $\mathbf{R}$. This discussion clearly illustrates that the left (or range space) Eigen vectors in $\mathbf{U}$ can indeed be used as optimal template features for distinguishing classes/targets. The number of u's to be chosen for classification depends on the distribution of λ.

4.2.2 Advantages with Eigen-Template based ATR

There are several key advantages in using eigen-templates as target features. Firstly, from minimum Mean-Squared Error context it has been theoretically shown above

that the eigen-vectors of the correlation matrix corresponding to the larger singular values are the *optimal* choice for feature selection. It may be observed from (4.5) that the range-space (or left) eigen vectors produced by the SVD operation are indeed found from the correlation matrix of the training data. Secondly, Eigen-template formation via SVD involves finding a set of orthonormal basis vectors that best describe the sub-space projection of the target space. Furthermore, according to [37], if the range-profile vectors y are Gaussianly distributed, then the eigenvectors selected as features maximize the *entropy* or *information* in the underlying distribution. As discussed the next Chapter, the Power Transform operation is applied for Gaussianization of the range data. Hence, according to [37], since the basis eigenvectors are chosen for which the singular values (*i.e.*, the variances) are the largest, the directions specified by the eigenvectors are also the ones for which the vector is "most random" having the maximum entropy.

The SVD operation in numerically robust and it inherently *decouples* the target basis space (corresponding to the large singular values) from the noise or clutter sub-space (corresponding to smaller singular values). Furthermore, the range-space eigen-vector corresponding to the largest singular value contains the maximum orthogonal projection—*i.e.* information—from the range space of the target-sector under consideration. In addition, range-space eigen-templates produced by the SVD operation for all target classes are automatically normalized to the length of unity, regardless of the signal strength of radar return. Hence, it can be concluded that information on the differences between target classes is contained within the amplitude variations in the range profiles.

Another advantage of the normalized eigen-template based approach is that Matched filtering (or location of maximum correlation) gives the optimum result, no on-line least-squares matrix-inverse operation is necessary to account for scaling

and/or dc-shift [42] and Matched Filtering requires Normalized inputs [34]. It may also be emphasized here that Eigen-templates are formed off-line using training data and no on-line Eigen-decomposition is necessary. In work with Eigen-template based classification using the XPATCH database, significant and consistent improvement was observed when compared with ATR using Mean-templates. The results are summarized in Chapter 6.

4.3 Clutter Suppression Capability of SVD

One of the critical problems faced in ATR is Clutter noise that often corrupt the SAR images or HRR profiles. Noise suppression is a common problem faced in many different fields of radar, sonar, speech, image *etc.* [26]. In various radar and sonar applications, SVD has been found to be highly effective for noise suppression and also for improved estimation of underlying system parameters, *etc.* SVD or Eigen-Decomposition (also known as Karhunen-Loeve Transformation or Principal Component Analysis) has also been used for improved pattern recognition [3, 12]. The SVD operation projects the information content in a HRR profile matrix into orthogonal basis spaces. The basis spaces with larger (or, dominant) singular values correspond to the underlying "signal-subspace" whereas those corresponding to the smaller singular values would correspond to the "noise-subspace" (or, in case of SAR or HRR profiles, this will also include "clutter subspace"). Hence, in order to suppress or "get rid of" noise, a common approach has been to re-construct the original matrix, albeit after "zeroing-out" most of the "noise subspaces" - this approach is sometimes known as, "Eigen Filtering" or "Subspace Filtering" [3, 26]. Any ATR/D then can be accomplished using this Eigen-filtered HRR profile or SAR image, as the case may be. As described in section 4.2 and shown in figures 4.5 and 4.6, SVD analysis of HRR profiles for both XPATCH and raw MSTAR data indicated significant energy

contributions from a very small number of signal-subspace vectors. Figures 4.3 and 4.5 show that only 1 eigen value accounts for more than 90% of the distribution power for both data types.
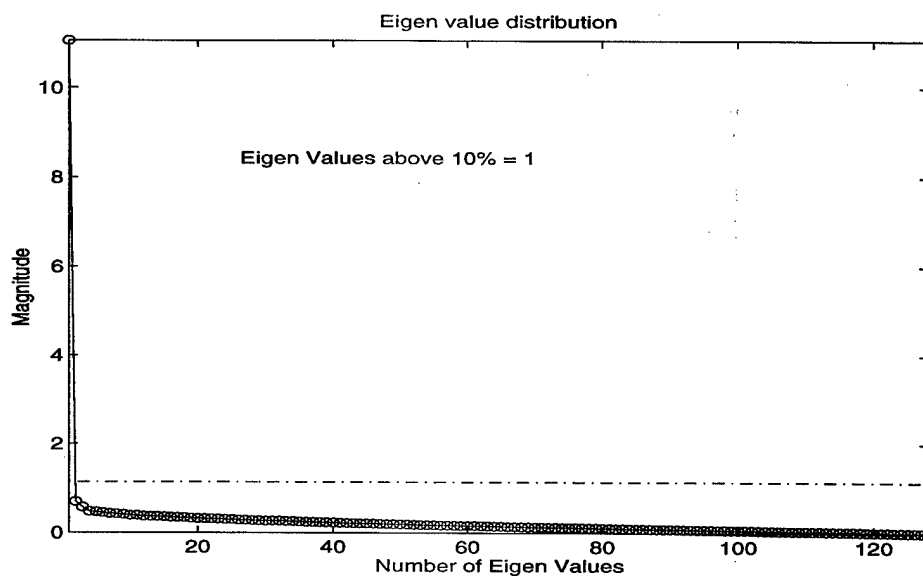

Figure 4.5: Distribution of Singular values for MSTAR data set, Target type: T72-132, Elevation: 17°, Aspect: 36.79°, $v = 0.2$
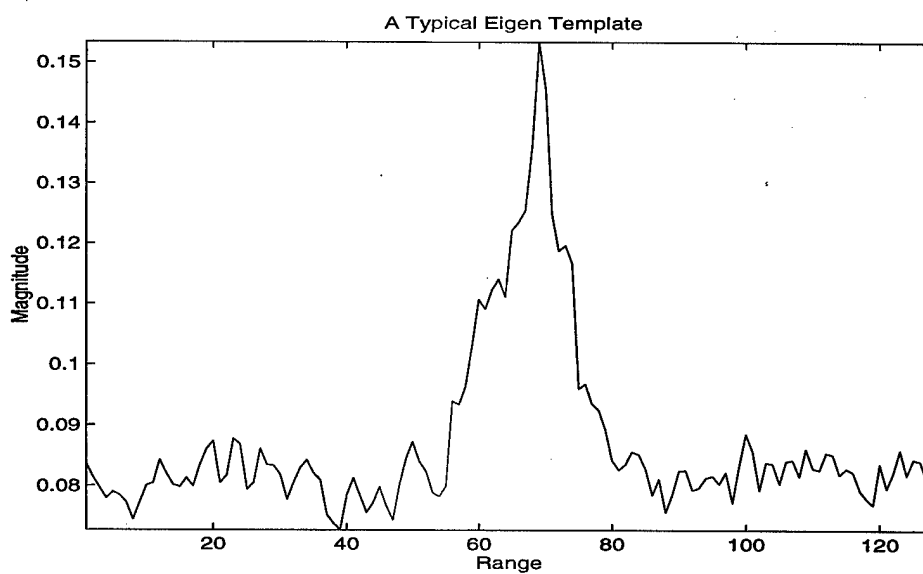

Figure 4.6: A typical Eigen template for MSTAR data set, Target type: T72-132, Elevation: 17°, Aspect: 36.79°, $v = 0.2$

For a HRR profile matrix $\mathbf{Y}$

$$\mathbf{Y} = \sum_{i=1}^{M} \lambda_i \mathbf{u}_i \mathbf{v}_i^T \qquad (4.20)$$

Equation (4.20) represents the eigen reconstruction using optimal features, which in turn depends on the dominant singular values. For both XPATCH and MSTAR database HRR profiles, λ_{11} accounted for more than 90% power of the distribution, as shown in figures 4.3 and 4.5.

Figures 4.7, 4.9, 4.11 and 4.13 show the HRR reconstruction using only first singular value of the distribution for XPATCH targets M1, T72, SB and FT respectively. It is known for the data that the target is centered and in these figures all the useful information in the original HRR image is retained whereas the clutter appears to have been suppressed. In figures 4.8, 4.10, 4.12 and 4.14 reconstruction is done using 3 Singular values, the useful signal information content is not changed much but clutter also appears to be present. It is a known fact that if all the Eigen values are considered for reconstruction, the profile can be re-obtained. It can be clearly observed here that if appropriate number of eigen values are taken, in our case 1, then clutter can be easily suppressed by the eigen filtering technique. Figure 4.15 shows the HRR profile reconstruction using only first Eigen value of the original HRR profile for MSTAR data set. As is evident, the noise spikes reduce and this may tend to improve ATR performance. The target is known to be in the center of the original image and around it is the possible clutter caused due to surroundings *etc.* The difference between original and reconstructed HRR profile is minimum in the center, thereby illustrating that the maximum information of the target is being restored, whereas the clutter, caused to the surroundings, may be suppressed.

Figure 4.7: HRR Image Reconstruction using only λ_{11} for XPATCH data set, Target type: M1, Sector: 60° - 62.5°, $v = 0.08$ (a) Original HRR Image (b) HRR Image after Eigen Filtering (c) Clutter

Figure 4.8: HRR Image Reconstruction using λ_{11} through λ_{33} for XPATCH data set, Target type: M1, Sector: 60° - 62.5°, $v = 0.08$ (a) Original HRR Image (b) HRR Image after Eigen Filtering (c) Clutter
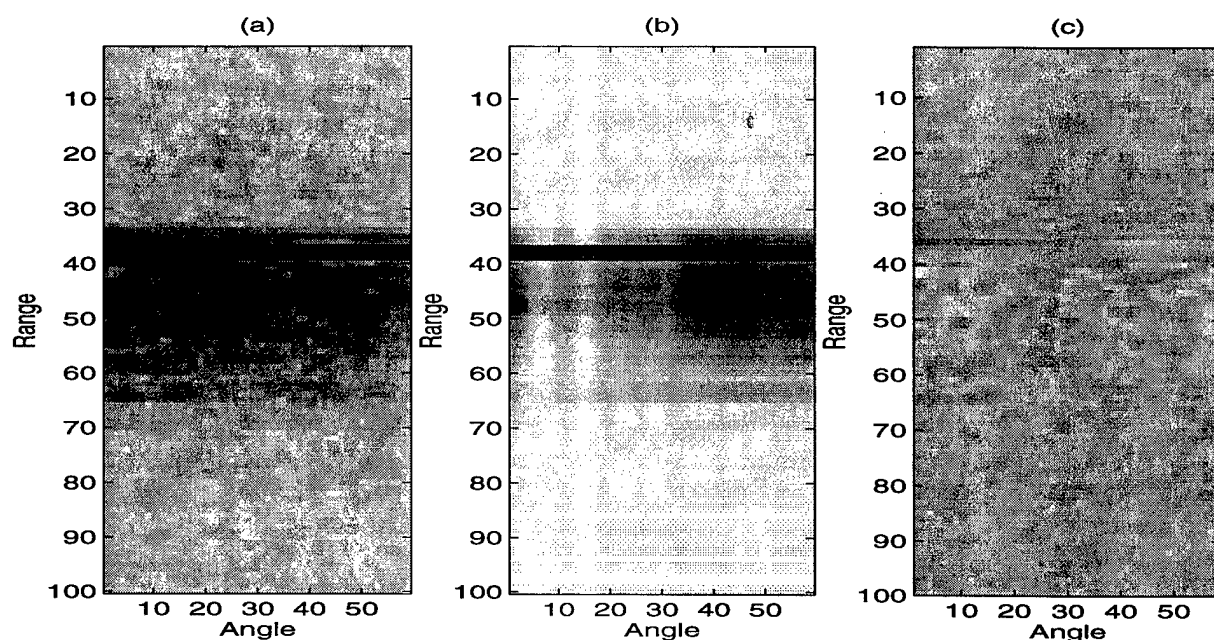
Figure 4.9: HRR Image Reconstruction using only λ_{11} for XPATCH data set, Target type: T72, Sector: $60°$ - $62.5°$, $v = 0.08$ (a) Original HRR Image (b) HRR Image after Eigen Filtering (c) Clutter

Figure 4.10: HRR Image Reconstruction using only λ_{11} through λ_{33} for XPATCH data set, Target type: T72, Sector: $60°$ - $62.5°$, $v = 0.08$ (a) Original HRR Image (b) HRR Image after Eigen Filtering (c) Clutter

Figure 4.11: HRR Image Reconstruction using only λ_{11} for XPATCH data set, Target type: SB, Sector: $60° - 62.5°$, $v = 0.08$ (a) Original HRR Image (b) HRR Image after Eigen Filtering (c) Clutter
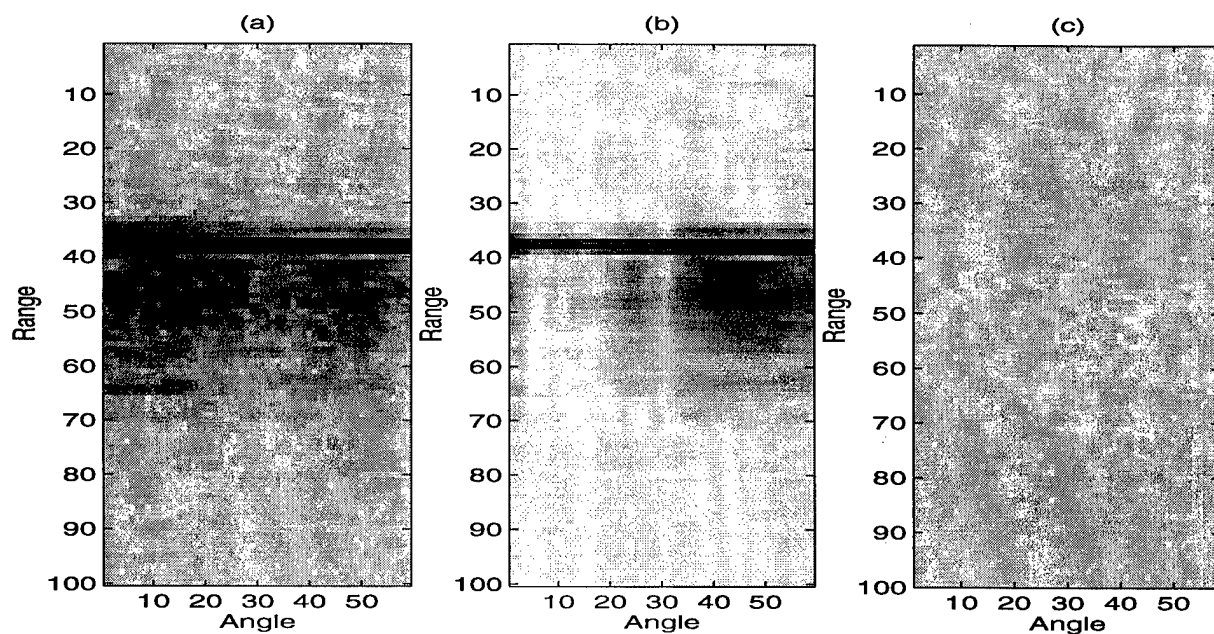

Figure 4.12: HRR Image Reconstruction using only λ_{11} through λ_{33} for XPATCH data set, Target type: SB, Sector: $60° - 62.5°$, $v = 0.08$ (a) Original HRR Image (b) HRR Image after Eigen Filtering (c) Clutter
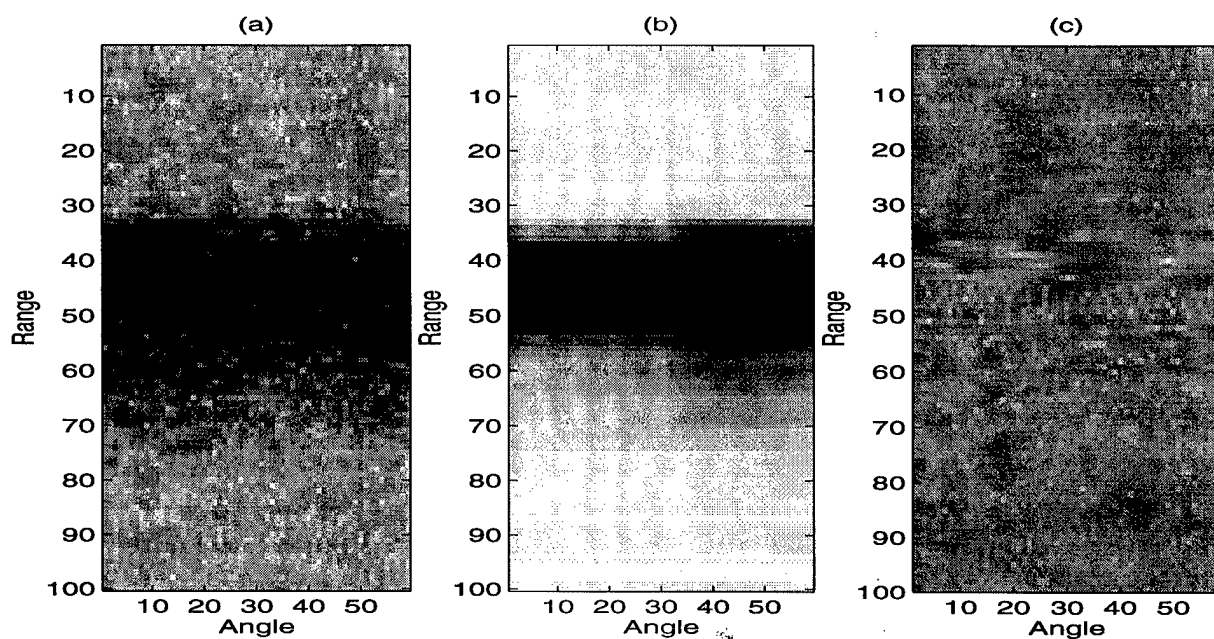
Figure 4.13: HRR Image Reconstruction using only λ_{11} for XPATCH data set, Target type: FT, Sector: 60° - 62.5°, $v = 0.08$ (a) Original HRR Image (b) HRR Image after Eigen Filtering (c) Clutter
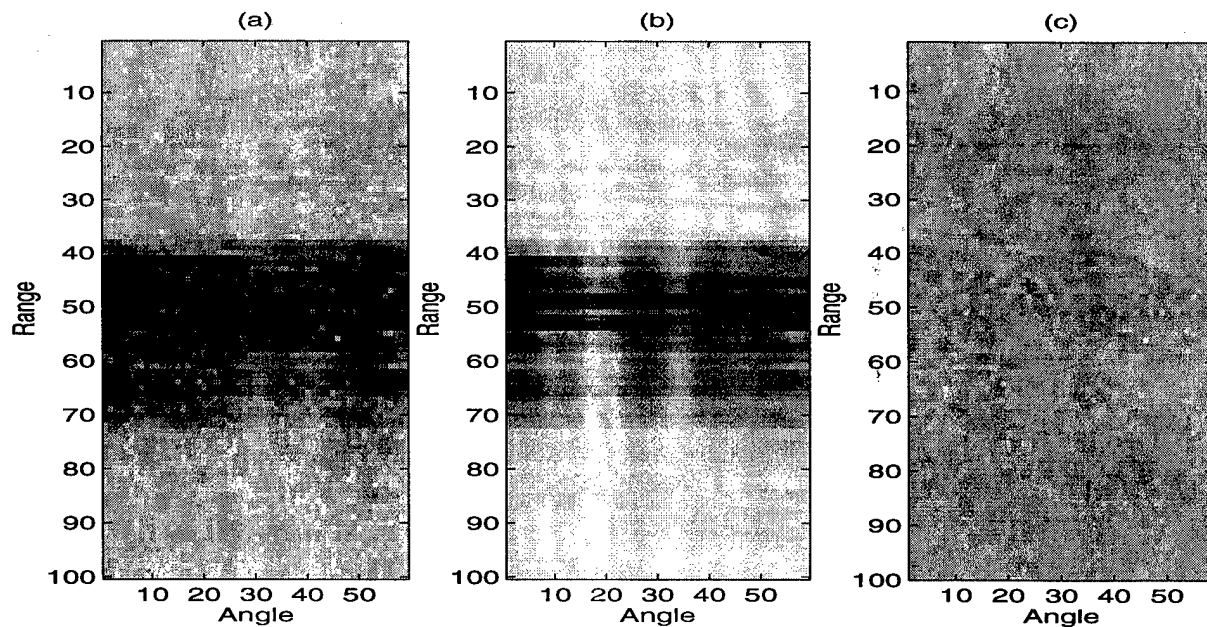
Figure 4.14: HRR Image Reconstruction using only λ_{11} through λ_{33} for XPATCH data set, Target type: FT, Sector: 60° - 62.5°, $v = 0.08$ (a) Original HRR Image (b) HRR Image after Eigen Filtering (c) Clutter
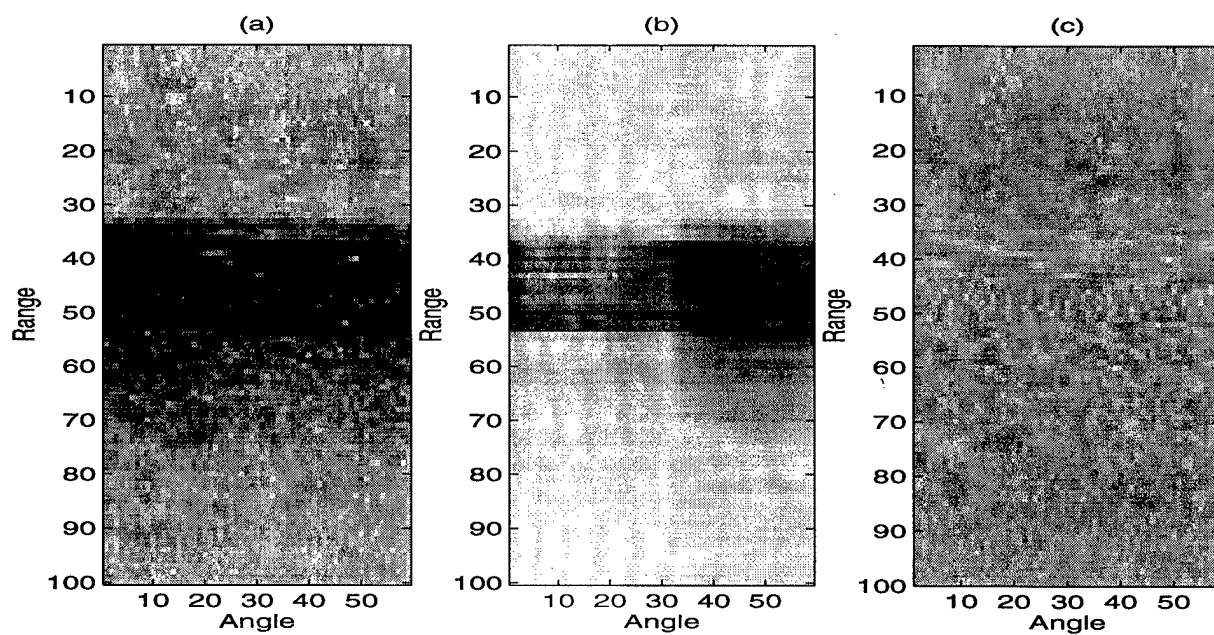
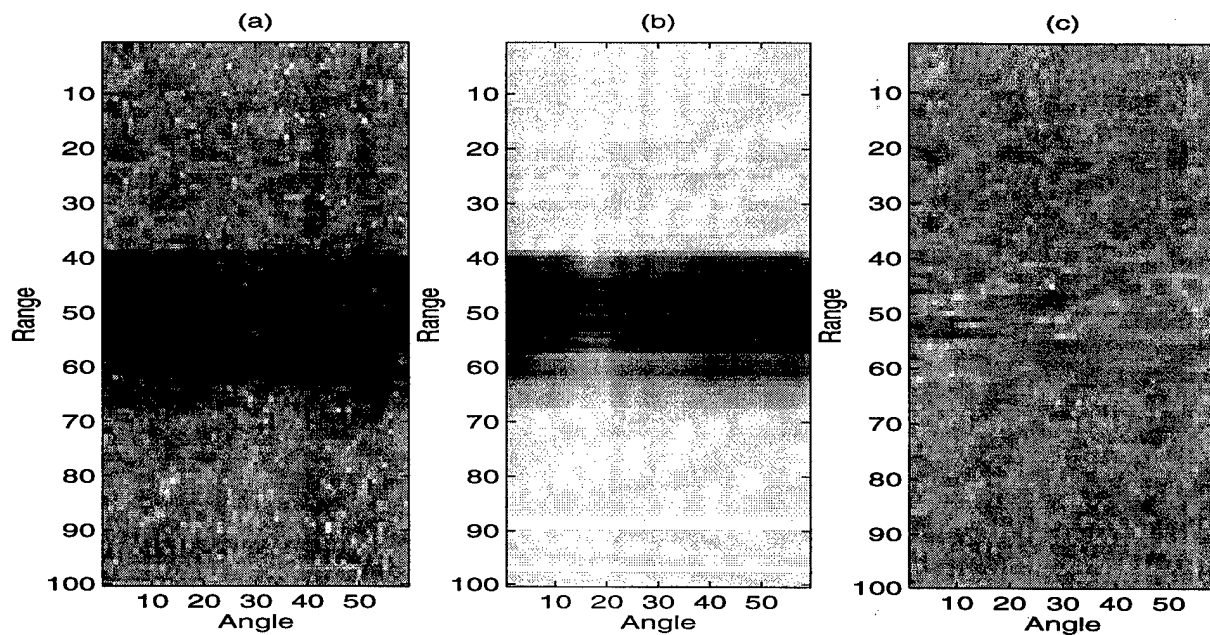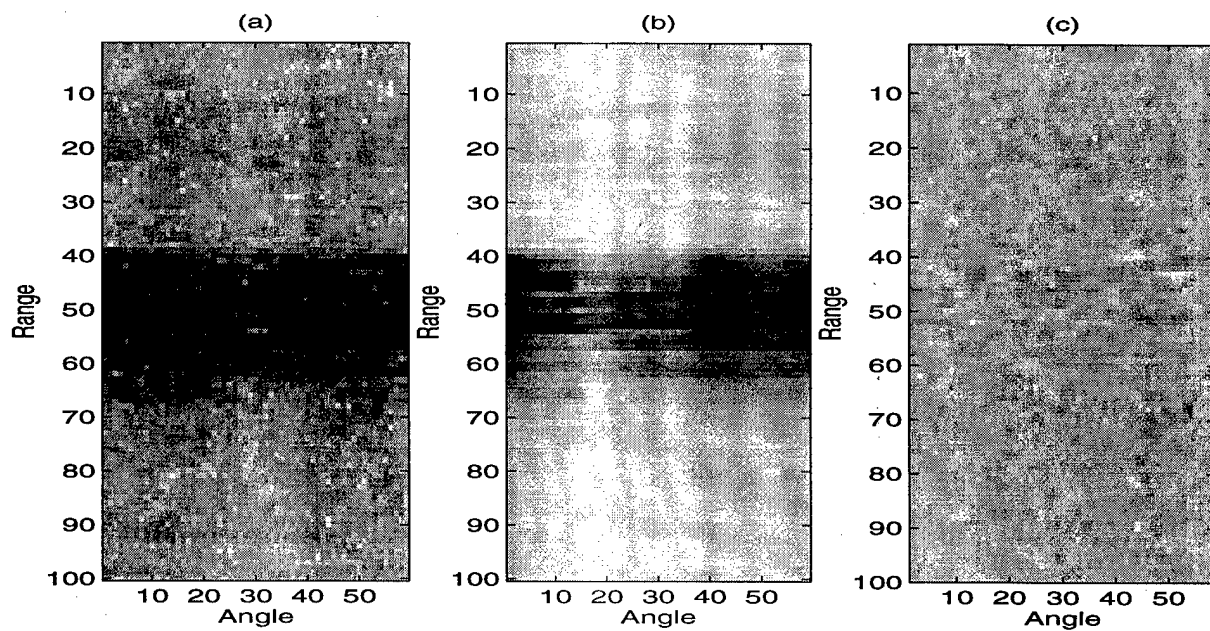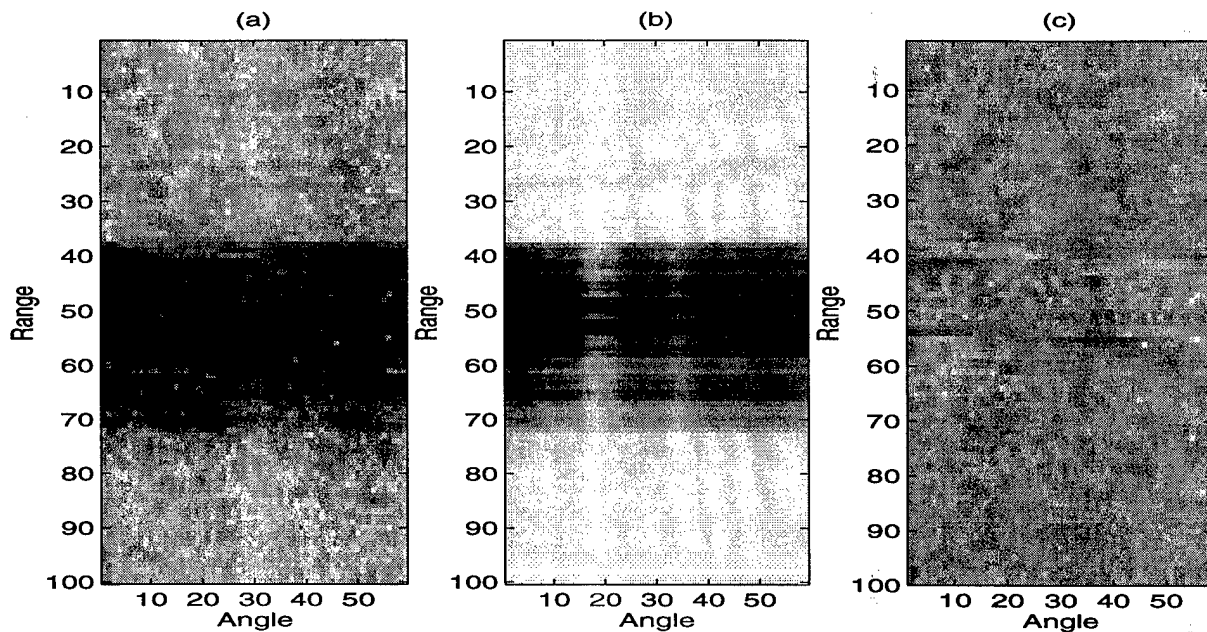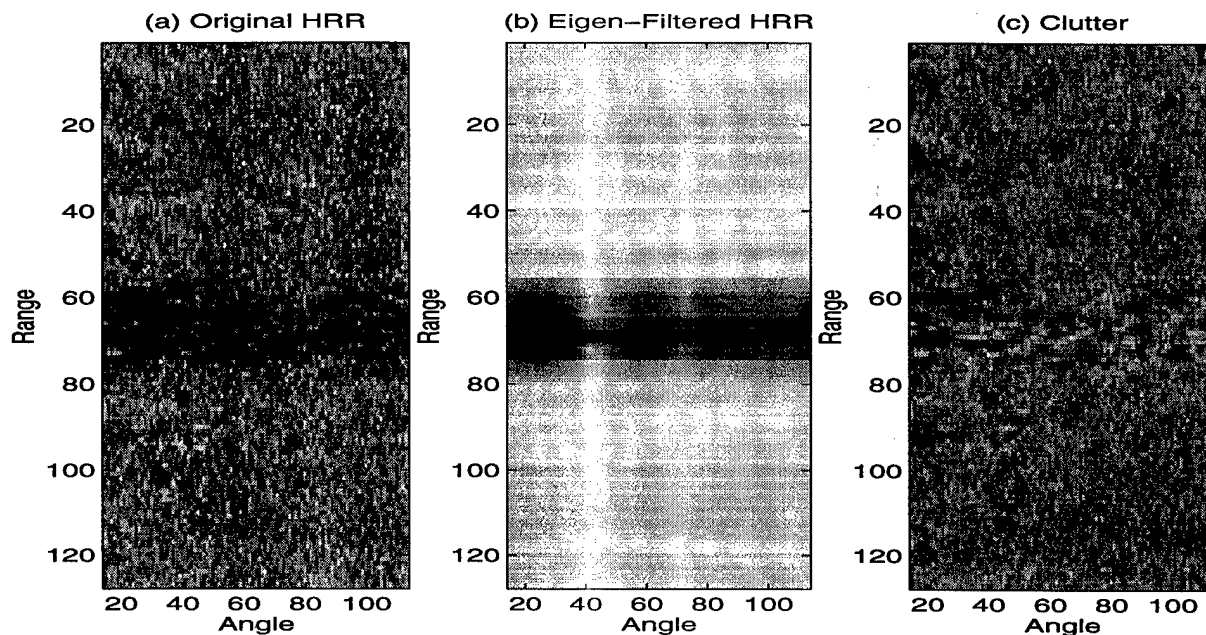Figure 4.15: HRR Image Reconstruction using only λ_{11} for MSTAR data set, Target type: T72-132, Elevation: 17°, Aspect: 36.79°, $v = 0.2$: (a) Original HRR Image (b) HRR Image after Eigen Filtering (c) Clutter

4.4 Target Classification

Given observed (or, test) range profile(s) of an unknown target, the ultimate objective of classification is to determine which target class it belongs to. This is accomplished by comparing the observed profile with all the available templates, which are assumed to have been formed beforehand using training data set. Two methods for recognition have been considered in this project, namely, *Least Squares* and *Matched Filtering*. Although these are standard techniques, brief discussions follow for completeness' sake.

4.4.1 Classification using Least Squares

For a given observation (or test) profile, the best template match is found in this case by minimizing the *mean squared error* (MSE) between the given test profile and its linear model using the template. Consider a test profile, **a**, and a template, **m**, of

equal sizes $L \times 1$. The linear model assumes that the observation (or test) profile can be modeled from the template by scaling and dc-level shifting as given by

$$\hat{\mathbf{a}} = z_1 + \mathbf{m}z_2 \tag{4.21}$$

$$= \begin{bmatrix} 1 & \mathbf{m} \end{bmatrix} \begin{bmatrix} z_1 \\ z_2 \end{bmatrix} \tag{4.22}$$

$$= \mathbf{J}\mathbf{z} \tag{4.23}$$

where, z_1 and z_2 represent the dc-level and scaling factor, respectively. These unknown constants are found for each template under consideration by minimizing the following squared error,

$$\min_{\mathbf{z}} \|\epsilon\|^2 = \|\mathbf{a} - \hat{\mathbf{a}}\|^2 \tag{4.24}$$

The solution to this least square problem is given by,

$$\hat{\mathbf{z}} = \mathbf{J}^{\#}\mathbf{a} \quad \text{where,} \quad \mathbf{J}^{\#} = (\mathbf{J}^T\mathbf{J})^{-1}\mathbf{J}^T \tag{4.25}$$

There are various ways to solve (4.25). Here, the problem was solved using the method of QR decomposition such that $\mathbf{J} = \mathbf{OP}$. From the property of QR-decomposition, $\mathbf{O}^T\mathbf{O} = \mathbf{I}$ and substituting in (4.25)

$$\hat{\mathbf{z}} = \mathbf{P}^{\#}\mathbf{O}^T\mathbf{a} \tag{4.26}$$

Once the estimate $\hat{\mathbf{z}}$, is obtained, the estimated profile is can be found as,

$$\hat{\mathbf{a}} = \mathbf{J}\hat{\mathbf{z}} \tag{4.27}$$

Using this $\hat{\mathbf{a}}$, the optimum MSE between the test profile and the estimated model ($\|\epsilon\|^2 = \|\mathbf{a} - \hat{\mathbf{a}}\|^2$) is calculated for each template in the training data set. The template having the minimum MSE is chosen as the matched target.

4.4.2 Matched Filtering

Let, H_0, H_1, H_2 and H_3 represent hypotheses that one among the four targets (M1, T72, FT and SB) in the XPATCH database is present. Let, the observation (or, test) and template profiles be denoted again by $\mathbf{a} = [a_1, a_2, \cdots, a_N]^T$ and $\mathbf{m}_i = [m_{i1}, m_{i2}, \cdots, m_{iN}]^T$, respectively. Each Hypothesis may then be represented by,

$$H_i \ : \ \mathbf{a} = \mathbf{m}_i + \mathbf{v} \qquad i = 1, 2, 3, 4 \tag{4.28}$$

where, $\mathbf{v}$ represents the noise or clutter samples, which are assumed to be zero mean, gaussianly distributed and white for this discussion. Clearly,

$$E\{\mathbf{a}|H_i\} \ = \ \mathbf{m}_i \tag{4.29}$$

$$var\{a_k|H_i\} \ = \ \frac{N_0}{2} \tag{4.30}$$

$$f(\mathbf{a}|H_i) \ = \ \frac{1}{\sqrt{\pi N_0}} \exp\left[-\frac{\sum_{k=1}^{N}(a_k - m_{ik})^2}{N_0/2}\right] \tag{4.31}$$

The MAP decision rule will involve choosing the hypothesis H_i for which the *a posteriori* probability $P(H_i|\mathbf{a})$ is maximized. Using Bayes' rule, the decision rule then becomes

Accept H_i for which $P(H_i)f(\mathbf{a}|H_i)$ is maximized.

Assuming all the 4 targets are equally likely, this decision rule is equivalent to choosing H_i for which this decision rule is equivalent to choosing H_i for which $f(\mathbf{a}|H_i)$ is maximized, which in turn, is equivalent to choosing H_i if

$$\sum_{k=1}^{N}\left(a_k - m_{jk}\right)^2 \qquad j = 1, 2, 3, 4 \tag{4.32}$$

is minimized when $j=i$. Equation (4.32) is the Euclidean distance between the test profiles $\mathbf{a}$ and the templates, $\mathbf{m}_j$, so that the rule chooses the template closest to

the test profile. If all templates, $m_i(n)$, have equal energy *i.e.* they are Normalized (*i.e.*, $\mathbf{m}_j^T\mathbf{m}_j = 1 \ \forall j$), then the problem of minimizing over i in (4.32) reduces to the following decision rule:

$$\text{Accept } H_i \text{ for which } I_j = \sum_{k=1}^{N} a_k m_{jk} \qquad j = 1, 2, 3, 4 \qquad (4.33)$$

is maximized when $j = i$. Equation (4.33) is a simple implementation of matched filter as a correlation classifier. The decision determines the target type for which the correlation between with a given observation (or test) profile is maximized. If the test profile vector and template are represented as $\mathbf{a}$ and $\mathbf{m}$ respectively, then the correlation between them can be considered as the output of a linear filter. In practice, a given $\mathbf{a}$ is correlated with all the templates, $\mathbf{m}$'s in the training database. If $\mathbf{a}$ and all the $\mathbf{m}_i$'s are not aligned, the correlation may have to calculated with various lag values and the maximum correlation among all lags for each target type is obtained. For each target there are a large number of templates at different aspects. Hence, the maximum correlation value among all templates for each target is determined. This process is repeated for all target classes, with each class being assigned its maximum correlation out of all lags for all aspect angles. Finally, The target class having the maximum correlation value among all classes is termed the matched target class. In our simulations with XPATCH database, correlation lag values up to ± 4 were used because for this simulated data set is reasonably well aligned. This shift may be increased for measured data, if necessary.

The figures below compare various ATR performances, in terms of detection and error probabilities, for combination of Normalization (N), Matched Filtering (MF) and Least-Squares (LS) using either eigen-templates (denoted by SVD) or mean-templates (MEAN) for several Power Transform (PT) coefficients. Figure 4.16 clearly shows that performance of eigen templates with matched filtering used as classification is better than mean-templates when used with Least-Squares for classification. Figure

4.17 shows that performance with Mean-templates improve considerably if normalized data is used with Matched Filter as classifier.

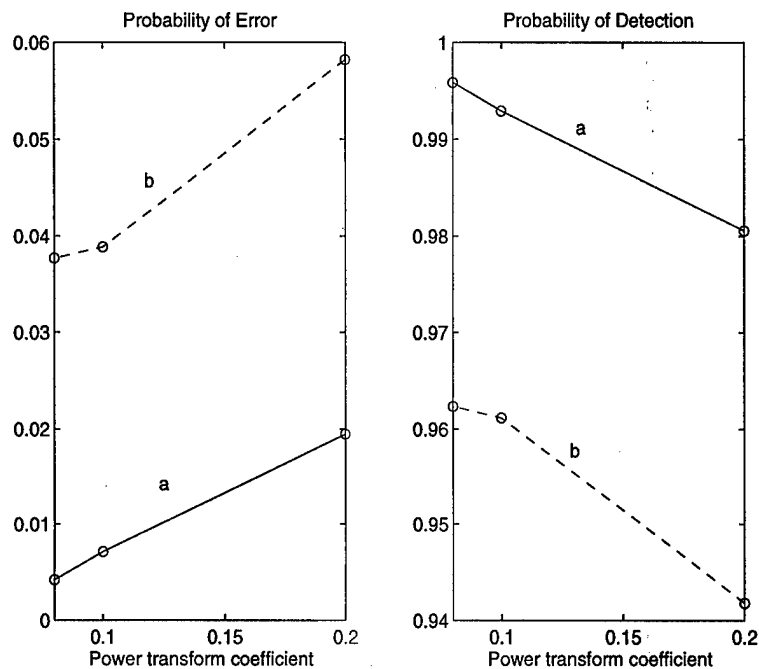Figure 4.16: Probability of Error and Probability of Detection for $v = 0.08$, 0.1 and 0.2 respectively for cases (a) Classification: PT+N+SVD+MF (b) Classification: PT+MEAN+LS
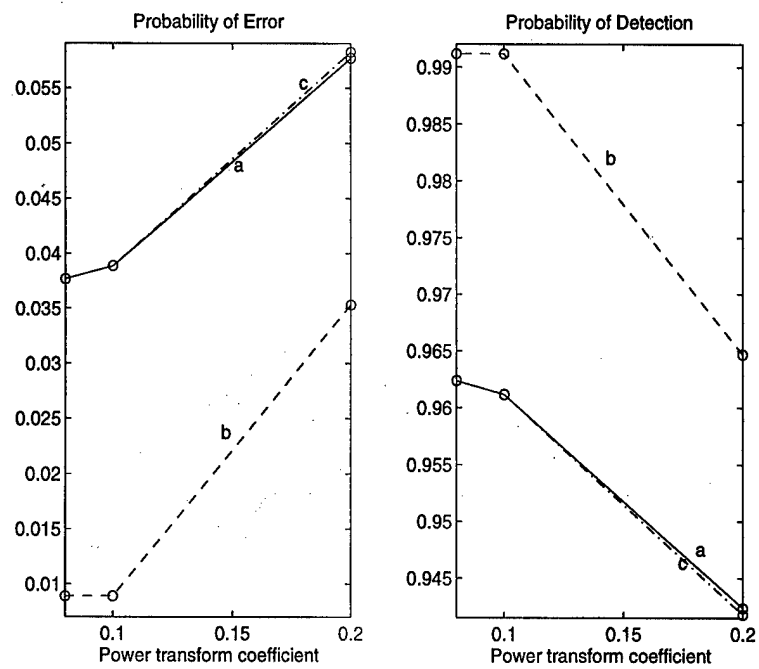
Figure 4.17: Probability of Error and Probability of Detection for $v = 0.08$, 0.1 and 0.2 respectively for cases (a) Classification: PT+N+MEAN+LS (b) Classification: PT+N+MEAN+MF (c) Classification: N+PT+MEAN+LS

Chapter 5

Tests for Gaussianity

As shown in Figure 3.2, Detected-HRR data are formed using absolute value of the Complex HRR data. Hence, Detected HRR is positive valued and tend to be Gamma or Rayleigh distributed for which optimum detection and estimation results are not usually straight-forward. On the other hand, many commonly used detection and estimation algorithms possess optimality properties for the Gaussian case [16]. As discussed in Chapter 3, it has been shown in [9] that certain distributions can be converted to close to normal by using a nonlinear mapping known as Power Transform (PT) of the data defined as,

$$Y = X^v, \qquad (0 < v < 1) \tag{5.1}$$

where, v denotes the PT-coefficient. It has also been shown in [9] that the Gaussianity property of Y enhances with reduction in the value of the PT-coefficient v Theoretical properties of the Power Transform mapping were thoroughly addressed in Chapter 3 (see section 3.1.3). In this Chapter we conduct numerical analysis on the HRR training data for testing the Gaussianity properties in order to determine appropriate values of v so as to achieve improved ATR performance.

5.1   Tests for Gaussianity

Two types of Tests were conducted to obtain the optimum value of the PT-coefficient, Chi-square Analysis [8, 11] and Bispectrum Analysis [25]. Chi-Square is a standard test for Gaussianity, whereas the Bispectrum based test exploits an important property of Gaussianity distributed random variables that their third-order moment as well as Bispectrum are theoretically zero [25]. Both tests were conducted for a set of values of v over an ensemble of HRR realizations [42]. The decision whether a realization is Gaussian or not was based on some pre-determined thresholds [8, 25]. Both tests indicated that the detected HRR data tend to be *more* Gaussian as the value of v is lowered, as predicted theoretically by Fukunaga. In Chi-square tests with XPATCH-HRR data, the optimum value of v was found to be 0.08, as depicted by Figure 5.1. This result was also corroborated by the Bispectrum based test.

5.1.1   Chi-Square Goodness-of-fit test for Normality

The goodness-of-fit tests are omnibus techniques that detect differences in kurtosis, location, skew, dispersion and so on. These statistic are often characterized as estimation-free or non-parametric. In case of Pearsons chi-square these are different as the marginal relative frequency f_j/N is used to predict the probabilities $P(x_j)$. The conditions that the distribution of any Pearsons chi-square statistic is approximated by $\tilde{\chi}^2(k)$ are

1. Each observation must fall into one and only one cell. In goodness-of-fit tests this means that the C columns define mutually exclusive categories

2. The N observations are independent of one another

3. The sample size N is large

The test is highly versatile and does not demand much exacting assumptions. In order to avoid the problem of normal distribution curve where there is small proportion of area under the tails, we define intervals associated with equal proportions of area under the normal curve. Each of these C cells are defined in such a way that each interval has a probability of $1/C$ under the normal curve. Given a vector to be tested for normality, the test can be summarized as follows [8]

1. Calculate the estimated mean and variance, μ and σ^2 respectively for that vector.

2. Choose C, the number of intervals, based on the conditions enumerated above.

3. Find the z values from the *Cumulative probabilities for the standard normal random variable* table corresponding to the upper limit of each interval. For the first interval, $\mathcal{P}(z) = 1/C$; for the second interval, $\mathcal{P}(z) = 2/C$; and so on. The last interval (like the first interval) is open ended. Here $\mathcal{P}$ is the cumulative probability.

4. Calculate the x-values of the class limits using μ and σ^2 calculated in step 1 and z value calculated in step 3 and substituting in equation (5.2).

$$x = \mu + z\sigma \qquad (5.2)$$

5. Based on the value of x found from equation (5.2), calculate the density function or in turn frequency distribution in these intervals. This observed frequency distribution is called f_j.

6. Calculate the expected frequencies. Every interval is associated with the same proportion (1/C), so the expected frequency in every interval is

$$F = N/C \qquad (5.3)$$

where N is the total number of observations, the length of the vector here.

7. Pearsons $\tilde{\chi}^2$ is calculated using equations (5.4) and (5.5).

$$F_j = Np_j \qquad (5.4)$$

$$\tilde{\chi}^2 = \sum_j^C \frac{(f_j - F_j)^2}{F_j} \qquad (5.5)$$

8. Based on the value of $\tilde{\chi}^2(k)$, found from step 7, and k, where k is the degrees of freedom, the cumulative probability is found, **p**. Here, $k = C - 3$ as μ and σ^2 are estimated mean and variance of the vector.

9. Based on the data analysis, a threshold value is decided.

10. If $1 - $ **p** is less than the threshold, then the signal is accepted as normal, else the normal hypothesis is rejected.
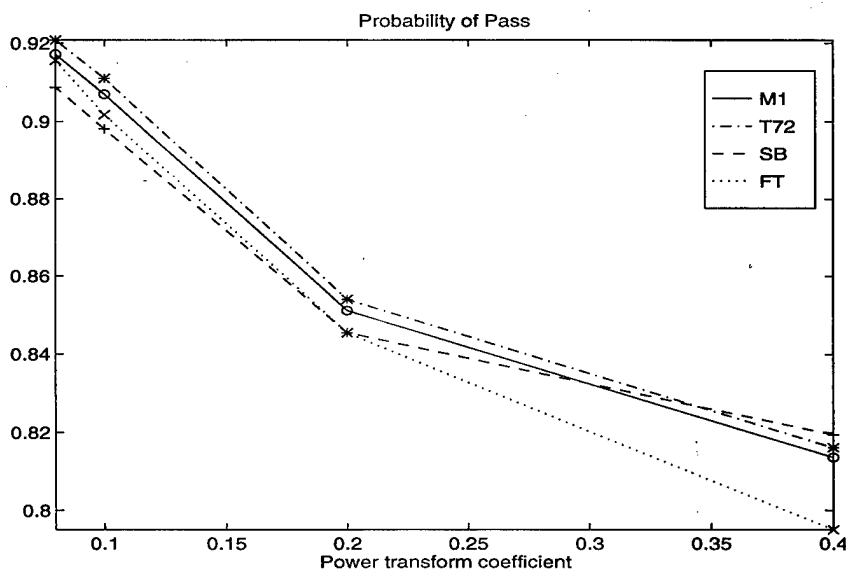

Figure 5.1: Probability of passing the Chi-Square test

5.1.2 Bi-spectrum Analysis

The theory of Bispectrum Analysis exploits an important property of Gaussianly distributed random variables that their third-order moment as well as Bispectrum are theoretically zero [31, 25]. It is shown below that this is true for all Gaussianly distributed random variables. Considering a multivariate Gaussian density function having a joint characteristic given by [31]

$$
\begin{aligned}
\mathbf{\Psi_x}(\omega_1, \omega_2, \cdots, \omega_n) &= E\left\{\exp\left[j(\omega_1 X_1 + \omega_2 X_2 + \cdots \omega_n X_n)\right]\right\} \\
&= \exp\left[j\mu_{\mathbf{x}}^{\mathbf{T}}\omega - \frac{1}{2}\omega^{\mathbf{T}}\Sigma_{\mathbf{x}}\omega\right]
\end{aligned}
\tag{5.6}
$$

where $\omega^T = (\omega_1, \omega_2, \cdots, \omega_n)$. The third moment of X can be obtained by

$$
E\{X_1, X_2, X_3\} = \frac{\partial^3 \mathbf{\Psi_x}(\omega_1, \omega_2, \omega_3)}{\partial \omega_1\, \partial \omega_2\, \partial \omega_3} \qquad at \quad \omega = 0
\tag{5.7}
$$

Taking $\mu_{\mathbf{x}}^T = 0$ in equation (5.6),

$$
\begin{aligned}
\mathbf{\Psi_x}(\omega_1, \omega_2, \omega_3) &= e^{-\frac{1}{2}\omega^T \Sigma_{\mathbf{x}} \omega}
\end{aligned}
\tag{5.8}
$$

$$
= 1 - \frac{1}{2}\omega^T \Sigma_{\mathbf{x}} \omega + \frac{1}{8}(\omega^T \Sigma_{\mathbf{x}} \omega)^2 + \cdots
\tag{5.9}
$$

Equation (5.9) represents the Taylor series expansion of (5.8). The higher order terms, having sixth and higher power of ω, are neglected. It is to be noted from (5.9) that the only non-zero term would be a term proportional to $\omega_1 \omega_2 \omega_3$, after taking partial derivative of (5.9) and setting $\omega_1 = \omega_2 = \omega_3 = 0$. The only non-zero term would come from the third term in (5.9) containing,

$$
(\omega^T \Sigma_{\mathbf{x}} \omega)^2 = \{\sigma_{11}\omega_1^2 + \sigma_{22}\omega_2^2 + \sigma_{33}\omega_3^2 + 2\sigma_{12}\omega_1\omega_2 + 2\sigma_{13}\omega_1\omega_3 + 2\sigma_{23}\omega_2\omega_3\}^2
\tag{5.10}
$$

The first three terms in (5.10) include the ω_i^2 terms. Hence, these are always zeros when ω_2's are set to zeros. All other terms also contain at least one higher power of ω_i. Clearly, the right hand side of (5.9) has no terms with $\omega_1\omega_2\omega_3$. Hence, the right hand side of equation (5.9) must equal to 0. The Bispectrum test for Gaussianity utilizes this unique property of Bispectrum which is true for any gaussian process. The test for Gaussianity is based on the theory of *oscillatory* stochastic processes, and as shown by Priestley and Subba Rao [25], it is closely related to the test for non-stationarity of a time series.

Let $\{B_k\}$ have a linear representation

$$B_k = \sum_{r=-\infty}^{\infty} a_r e_{k-r} \tag{5.11}$$

where $\{e_k\}$ is a sequence of *i.i.d* random variables. The auto-covariance function is defined as

$$
\begin{aligned}
\mathbf{R}(s) &= E[B_k B_{k+s}] \\
&= E\left[\left(\sum_{r=-\infty}^{\infty} a_r e_{k-r}\right)\left(\sum_{r'=-\infty}^{\infty} a_{r'} e_{k+s-r'}\right)\right] \\
&= \sum_{r}\sum_{r'} a_r a_{r'} E[e_{k-r} e_{k+s-r'}]
\end{aligned}
\tag{5.12}
$$

As e_k's are independent, equation (5.12) reduces to

$$\mathbf{R}(s) = \sigma^2 \left[\sum_{r=-\infty}^{\infty} a_r a_{r+s}\right] \tag{5.13}$$

The third order central moment of $\{B_k\}$ is

$$
\begin{aligned}
C(k_1, k_2) &= E[B_k B_{k+k_1} B_{k+k_2}] \\
&= \sum_{r_1}\sum_{r_2}\sum_{r_3} a_{r_1} a_{r_2} a_{r_3} E[e_{k-r_1} e_{k+k_1-r_2} e_{k+k_2-r_3}]
\end{aligned}
$$

$$= \mu(\sum_r a_r a_{r+k_1} a_{r+k_2}) \qquad (5.14)$$

$H(w)$ is defined as the transfer function of equation (5.11) of the type

$$H(w) = \sum_{r=-\infty}^{\infty} a_r e^{-ir\omega} \qquad (5.15)$$

Then the spectral and Bi-spectral density functions [15] for $\{B_k\}$ are

$$
\begin{aligned}
f(w) &= \frac{1}{2\pi} \sum_{s=-\infty}^{\infty} \mathbf{R}(s) e^{-is\omega} \\
&= \frac{\sigma^2}{2\pi} |H(\omega)|^2 \qquad (5.16)
\end{aligned}
$$

$$f(\omega_1, \omega_2) = \frac{\mu}{2\pi^2} H(\omega_1) H(\omega_2) H(-\omega_1 - \omega_2) \qquad (5.17)$$

Based on this, B_{ij} can be defined as

$$
\begin{aligned}
B_{ij} &= \frac{|f(\omega_i, \omega_j)|^2}{f(\omega_i) f(\omega_j) f(\omega_i + \omega_j)} \\
&= \frac{\mu^2}{2\pi\sigma^2} \qquad (5.18)
\end{aligned}
$$

i.e. B_{ij} is independent of ω_i and ω_j. Based on this theory, the following hypothesis is defined

1. H_0 : $f(\omega_i, \omega_j) = 0$, for all ω_i and ω_j; and

2. H_1 : B_{ij} is constant for all ω_i and ω_j

Acceptance of H_0 is only consistent with linearity and $\mu = 0$. Acceptance of H_1 and rejection of H_0 implies that the process is not Gaussian but consistent with being linear. A test vector is taken and on the basis of the above equations, the Hotelings

T^2 value is obtained and using the hypothesis, it is decided whether a vector has normal density or not.

Simulation results on both Chi-square and Bispectrum-based tests for Gaussianity are included in the next Chapter.

Chapter 6

Simulations

6.1   HRR profile generation

The four target XPATCH database contains simulated radar returns at 100 frequencies per look-angle with angular resolution between adjacent looks being $0.04°$. Hence, encompassing the entire $360°$ of look angles, the XPATCH generated CPH matrices are of size 100×9000 for each target. The test profiles as well as the templates were obtained from this matrix. As the test profile could be corresponding to any aspect angle, every $20th$ Angle was retrieved in the form $1, 21, 41, \cdots$, and stored as the test profiles in CPH mode, matrix $\mathbf{A}$ of size 100×425, where 100 and 425 represent the number of Range gates and Angles or looks respectively. The remaining matrix was divided into 144 non-overlapping sectors with each sector encompassing $2.5°$ of look angles, each sector being of size 100×59, where 100 and 59 are the Range gates and looks within a single sector.

Each one of these 144 sectors has to be converted from the CPH to the HRR profiles. As shown in Figure 3.2, HRR data (Range $vs.$ Angle) is formed by performing 1-D FFT in the frequency domain to generate the range information. This process involves taking the Fourier transform of all the Range profiles independently. At this stage the HRR profile for a sector is available, denoted by $\mathbf{X}$.

63
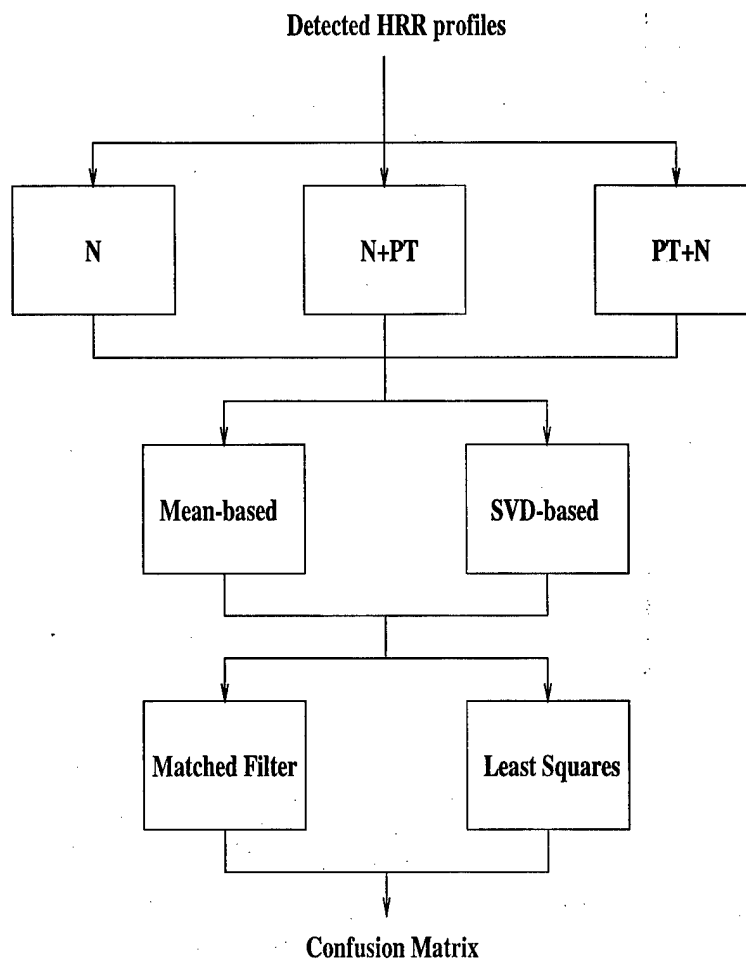
Figure 6.1: ATR algorithm block diagram

6.2 Preprocessing

Figure 6.1 shows the three different possible combinations of Pre-processing, *viz.*

1. Power transform only (PT)

2. Power transform followed by Normalization (PT+N)

3. Normalization followed by Power transform (N+PT)

The following explanation is for case 2 above however the other two cases can be obtained by either neglecting the Normalization process or changing the sequencing of events.

The power transform of **X**, size 100×59, can be done by taking each and every Range profile and applying Equation (3.1) on it. The value of v in equation (3.1) is found through the Gaussianity tests explained below.

6.2.1 Test of Gaussianity

In Chapter 5, the test of Gaussianity were discussed, wherein the objective was to find a value for v in equation (3.1) such that maximum vectors have normal density function after application of Equation (3.1) on them. The Chi-square and Bispectrum based tests were performed on the power transformed HRR profiles of XPATCH data to obtain the optimum value of the power transform coefficient v.

Chi-square test for Normality

The data was Fourier transformed to form the HRR profiles, after formation of sectors, as discussed in section 6.1. The Chi-square Analysis was done over 14400 vectors, as each sector has 100 Range gates and 144 sectors are available per target. The result in Table 6.1 was obtained for various power-transform coefficients. The threshold was set to 0.05 for all analysis. As observed, the best value of power transform coefficient is 0.08. The same is felt from Figures 4.16, 4.17 and ATR P_e and P_D values. This was also realized from Figure 3.3, wherein more Gaussianity was expected by lowering v, which is evident through Table 6.1

Bispectrum Analysis

Based on the theory explained in section 5.1.2, the Hoteling's T^2 value was computed. Bispectrum analysis is highly computational and this is a major drawback with it. Considering this issue, instead of performing the test over 14400 vectors, a smaller ensemble of 20 vectors was chosen and Hoteling's T^2 value was computed for profiles that were power transformed with $v = 0.08$, 0.1 and 0.2. Instead of fixing a threshold in case of Bispectrum, the ratio of the Hoteling's T^2 value was taken for different power

Power Transform Coefficient	Total Tests (Range Gates × Sectors)	M1	T72	SB	FT
0.4	14400	11717	11753	11801	11449
0.2	14400	12257	12298	12175	12174
0.1	14400	13061	13119	12933	12985
0.08	14400	13207	13259	13087	13185

Table 6.1: Comparison of Gaussianity results for various Power transform coefficients

transform coefficients. The main analogy behind it was the more the Gaussianity, the lower the Hoteling's T^2 value.

$$\gamma = \frac{T^2 \text{ value with } v = 0.08}{T^2 \text{ value with } v = 0.1} \tag{6.1}$$

$$\gamma = \frac{T^2 \text{ value with } v = 0.08}{T^2 \text{ value with } v = 0.2} \tag{6.2}$$

As seen in figures 6.2 and 6.3, the ratio of there corresponding T^2 values, γ of (6.1) and (6.2) respectively, showed that more vectors being Gaussian for $v = 0.08$ as compared with 0.1 and 0.2. Although it was not possible to carry out this test on all vectors, the results in figure 6.2 and 6.3 indicate relatively consistent better performance with $v=0.08$. Hence, the optimum value of v for good ATR results was chosen as 0.08.

After performing the power transform operation, power transformed HRR profiles are obtained, denoted by **Y** (size 100×59). The process of Normalization is carried out similarly by taking each and every Range profile and setting the length, or norm, of the vector to unity as shown in (6.3).
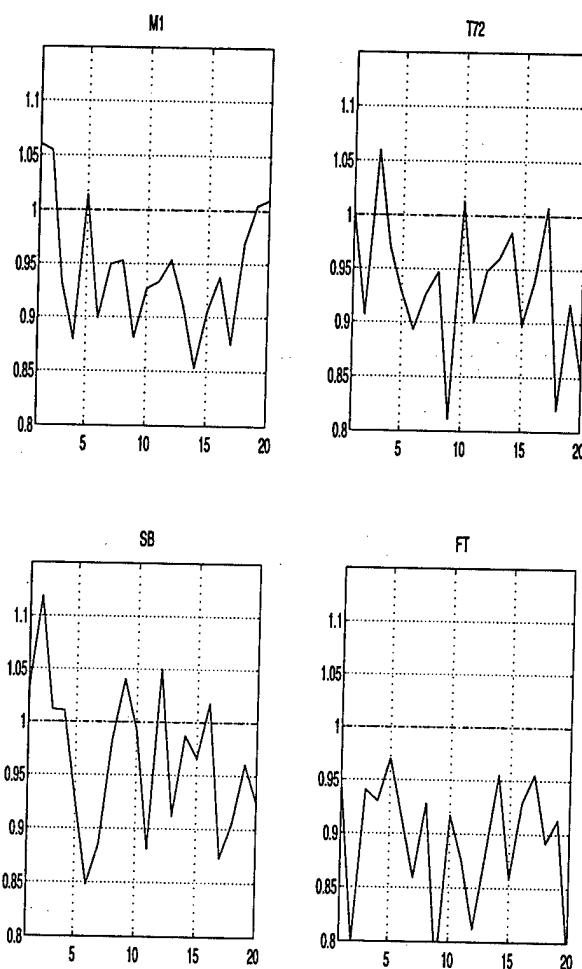
Figure 6.2: Ratio of Hoteling's T^2 test for $v = 0.08$ to $v = 0.1$

$$\mathbf{y}_{normalized} = \frac{\mathbf{y}_{unnormalized}}{\sqrt{y_1^2 + y_2^2 + \cdots + y_n^2}} \tag{6.3}$$

These operations do not affect the size of the matrix $\mathbf{Y}$ (100×59).

6.3 Feature extraction

Following the Pre-processing stage is the Feature extraction, which can be either mean-based or Eigen based. The two basis for feature extraction can be implemented as
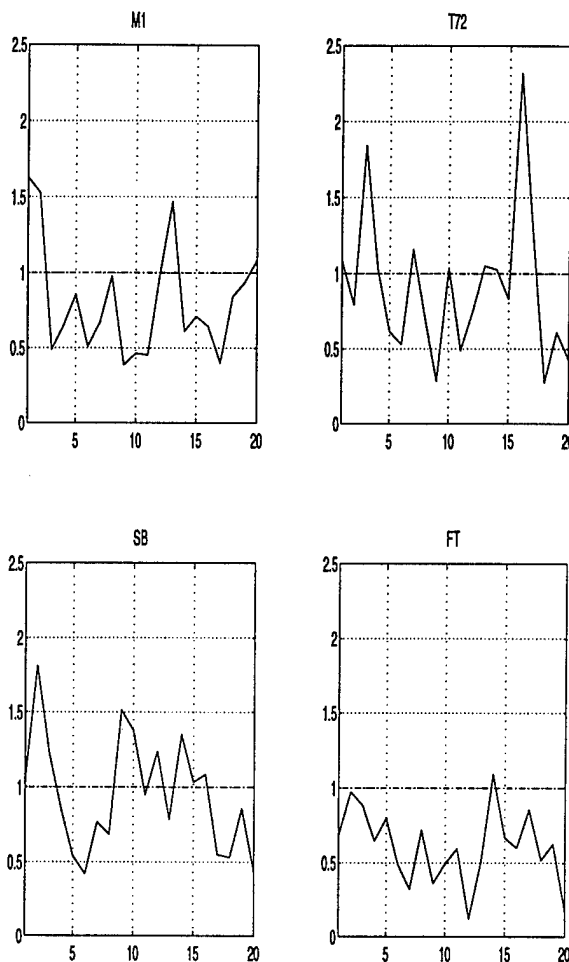
Figure 6.3: Ratio of Hoteling's T^2 test for $v = 0.08$ to $v = 0.2$

- **Mean Based:** Currently, one of the most common approaches for HRR Template formation is via averaging of the range profiles over a section of contiguous aspect angles and these are called Mean-Templates [42]. In this case, Power Transform with PT coefficient $v = 0.2$ had been applied to the detected HRR profiles before forming the mean templates. However, the template vectors for all classes were not normalized to the same length. Since the Mean-Template energies may vary between target classes, ATR decisions are based on a Linear LS fit, with associated drawbacks.

This approach is fairly straight forward and can be done by taking mean of the

matrix $\mathbf{Y}$ over all the look angles available. $\mathbf{Y}$ has 59 look angles and when averaged over these, it gives us the optimal feature, denoted by $\mathbf{t}$, size 100×1.

- **Eigen Based:** The theory of SVD, of decoupling the matrix into Range and Angle space orthogonal matrices, is brought to use. The SVD of $\mathbf{Y}$ gives us three matrices *viz.* U, Λ and $\mathbf{V}$, as shown in equation (4.4). In section 4.3.1, it has been shown that the Eigen vectors corresponding to the m largest Eigen values be used for classification. Figures 4.3 and 4.5 show that for XPATCH and MSTAR database λ_{11} makes up for more than 90% power of the entire distribution. Based on these facts, $\mathbf{u}_1$, corresponding to λ_{11}, was used as the optimal feature. For simplicity, $\mathbf{u}_1$ is denoted as $\mathbf{t}$, size 100×1 in the later discussion.

The feature selection, either mean based or Eigen based $\mathbf{t}$, for a sector has been obtained. The same is performed on all the 144 sectors with each sector rendering a vector of length 100. With the completion of the feature extraction stage, $\mathbf{T}$, a 100×144 size matrix is available which is referred to as the *templates* matrix. The same is done for all the 4 targets.

The test profiles are created using the 100×425 matrix $\mathbf{A}$ obtained as described in section 6.1. using similar operations of HRR generation, Power transform and Normalization. A very important fact stands that the sequencing of events in Pre-processing of templates and test profiles must be exactly the same. As the process of HRR profile generation, power transform and Normalization have no affect on the matrix size, $\mathbf{A}$ would still be of size 100×425. The matrix $\mathbf{A}$, is nothing else but 425 different test profile vectors, or Range profiles, from different and equally separated aspect angles bunched together. The same happens with all the 4 targets. The important thing to be noted here is that *t*here is no need for SVD in generating the test profile matrix. This is an important factor as the method involves minimum

on-line computation time. Templates are made off-line, so SVD operation there is acceptable.

The above operation gives the test profile matrix **A**, one to be recognized, and the template feature set library, **T**.

6.4 Recognition

The above system comes to the Recognition stage which can be done by either Matched Filtering technique or Least Squares explained in Chapter 4. Each one of the 425 test profile is taken and matched, in turn correlated within a shift of ± 4, with every template, for all targets $(144 * 4)$. The template type, either M1, T72, FT or SB, giving the best match , or highest correlation value, is taken as the target recognized.

6.4.1 Confusion Matrix

Confusion matrix summarizes the classifier performance. Confusion matrix can be generated here by taking all test profiles into consideration. The test profile of a particular target type is chosen and based on the classifier, it is recognized as either one of the four targets. Table 6.2 shows the organization of a confusion matrix. Based on table 6.2, P_e and P_D are given by

$$P_e = \sum_{i=1}^{i=4} \sum_{\substack{j=1 \\ i \neq j}}^{j=4} P(C_i)P(C_j|C_i) \tag{6.4}$$

$$P_D = \sum_{i=1}^{i=4} \sum_{\substack{j=1 \\ i=j}}^{j=4} P(C_i)P(C_j|C_i) \tag{6.5}$$

where C_i stands for M1, T72, FT and SB for i = 1, 2, 3 and 4 respectively. As can be inferred from (6.4) and (6.5), if a test profile fails to match a template of the same target type, it accounts to Probability of error whereas if it does match, then it accounts

to the Probability of Detection. In order to minimize Probability of error, in turn maximize Probability of Detection, various tests were conducted which are described in Chapter 6. Across a row of a confusion matrix, the conditional probabilities must equal to 1. Table (6.2) describes the probability factors in a confusion matrix.

Classification	M1	T72	FT	SB
M1	$P(M1\|M1)$	$P(T72\|M1)$	$P(FT\|M1)$	$P(SB\|M1)$
T72	$P(M1\|T72)$	$P(T72\|T72)$	$P(FT\|T72)$	$P(SB\|T72)$
FT	$P(M1\|FT)$	$P(T72\|FT)$	$P(FT\|FT)$	$P(SB\|FT)$
T72	$P(M1\|SB)$	$P(T72\|SB)$	$P(FT\|SB)$	$P(SB\|SB)$

Table 6.2: Confusion Matrix, C, Organization

6.5 ATR Performance Comparison

Figures 6.4 and 6.5 show the ATR results using Mean templates in terms of Probability of Error (P_e) and Probability of Detection (P_D). The plots show the results without and then with template normalization, respectively, using Least-Squares (LS). Clearly, if LS is used normalization has very little effect. However, if Matched Filtering (MF) is used with normalized mean templates, the results improve significantly as shown by Figures 6.4(c) and 6.5(c). Figures 6.6 and 6.7 show the corresponding results using Eigen Templates. Once again, LS performs poorly regardless of normalization, whereas performance with MF is superior with normalized templates. Figures 6.4, 6.5, 6.6 and 6.7 demonstrate that ATR performance improves (*i.e.*, P_e reduces and P_D increases) as the PT coefficient v is reduced. It may be noted that Matched Filter performs quite poorly without normalization for both Mean and Eigen templates and hence, those results are not included here. According to Figures 6.4, 6.5, 6.6 and 6.7, the best results using Eigen and Mean templates are the ones which use Matched filtering with normalized templates. In Figures 6.8 and 6.9, these two cases

are compared separately to show that the performance of the eigen-based approach is superior than that of the Mean-based technique.
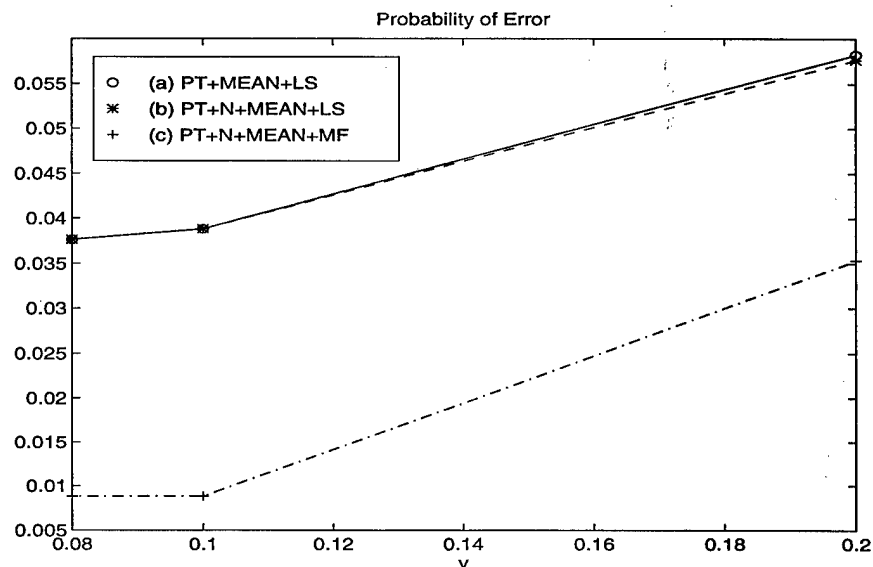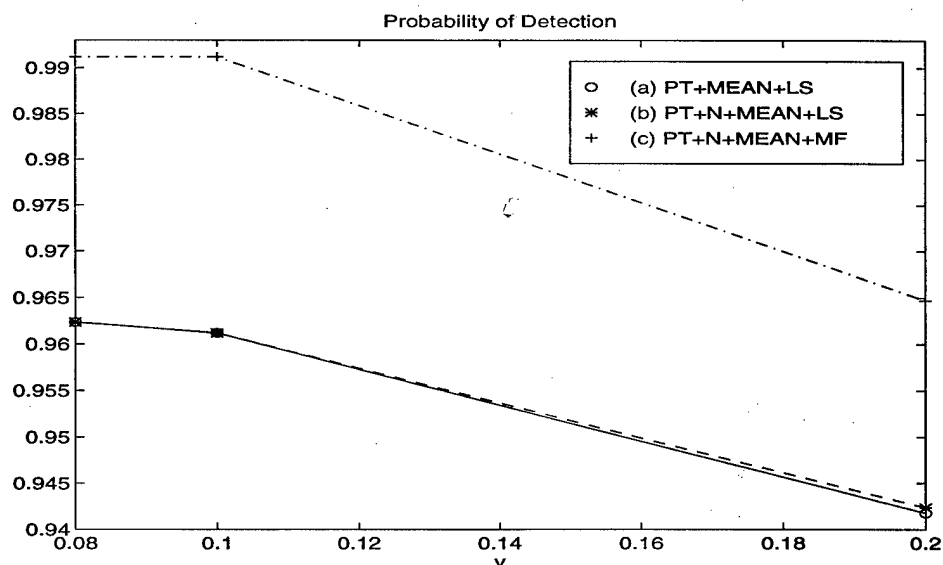

Figure 6.4: P_e using Mean Templates, (a) Least Squares without Normalization (b) with Normalization (c) Matched Filter with Normalization. $v = 0.08$, 0.1 and 0.2 for all cases.

Figure 6.5: P_D using Mean Templates, (a) Least Squares without Normalization (b) with Normalization (c) Matched Filter with Normalization. $v = 0.08$, 0.1 and 0.2 for all cases.
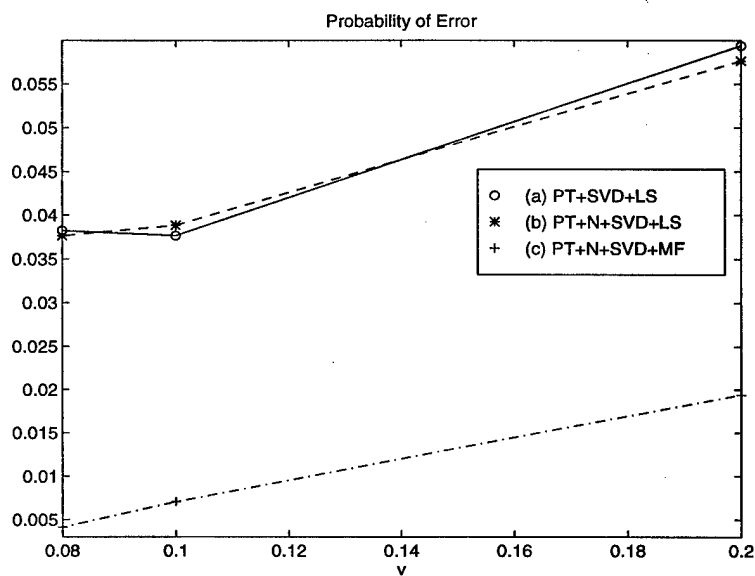
Figure 6.6: P_e using Eigen Templates, (a) LS without Normalization (b) with Normalization (c) MF with Normalization. $v = 0.08$, 0.1 and 0.2 for all cases.
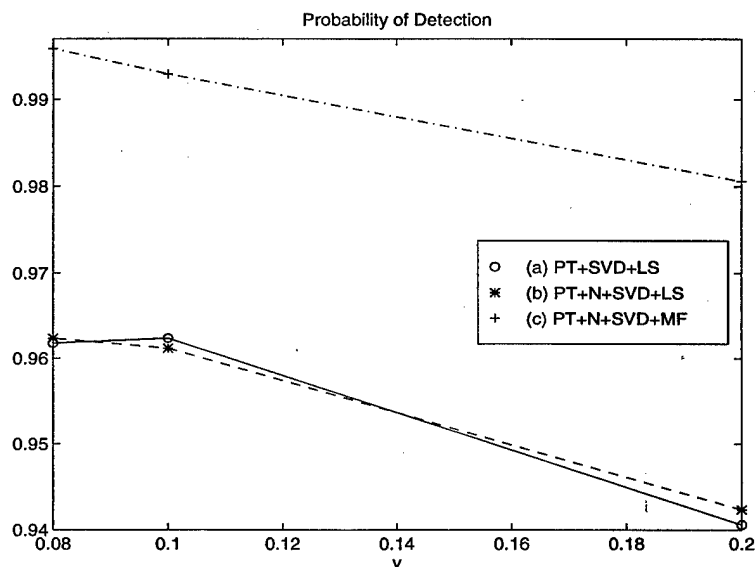

Figure 6.7: P_D using Eigen Templates (a) LS without Normalization (b) with Normalization (c) MF with Normalization. $v = 0.08$, 0.1 and 0.2 for all cases.
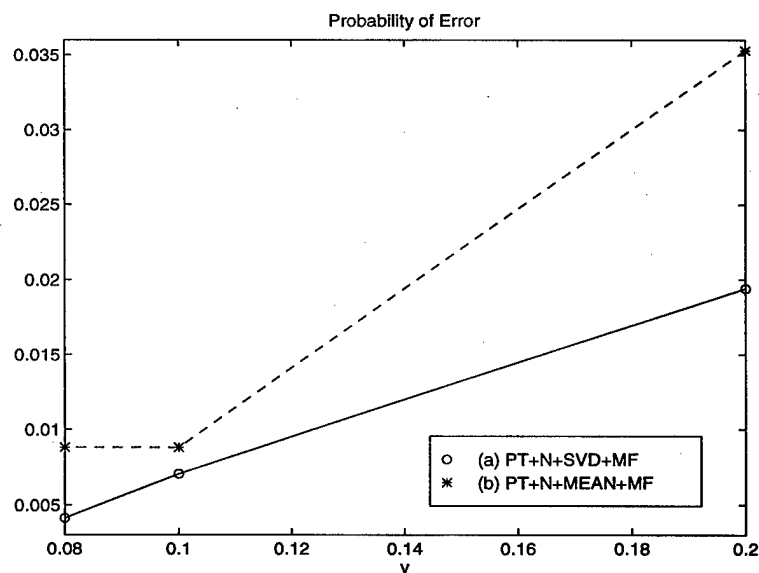
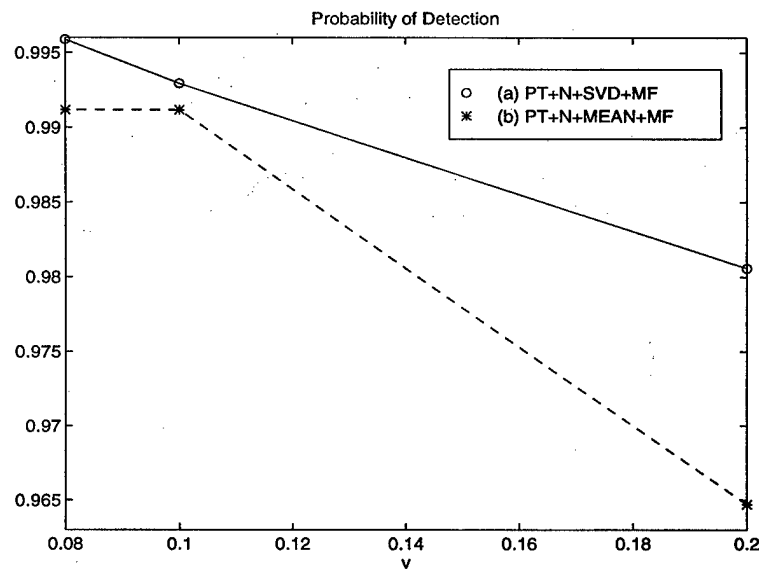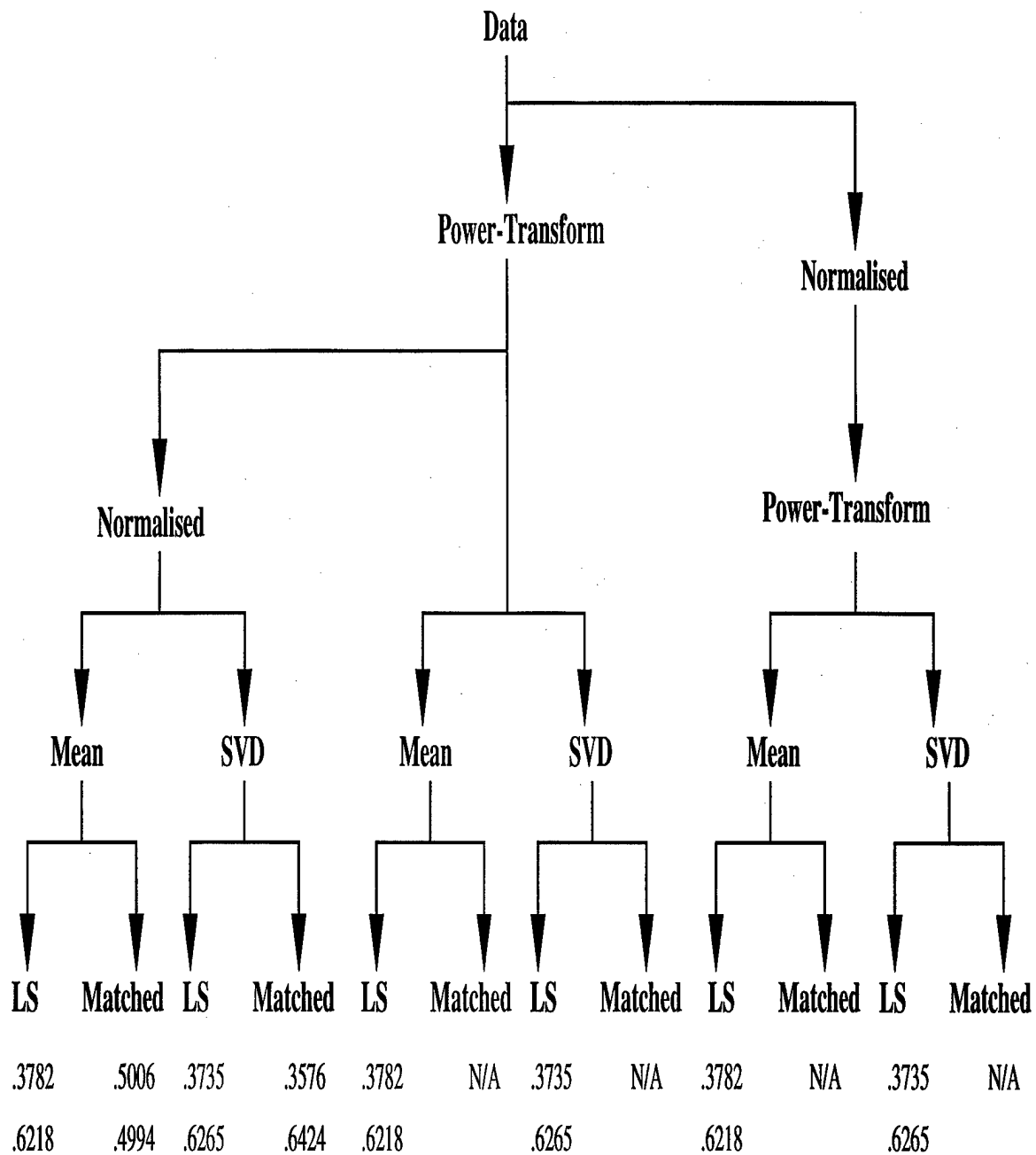Figure 6.8: Comparison of P_e performance using Matched Filter using (a) Eigen and (b) Mean templates.

Figure 6.9: Comparison of P_D performance using Matched Filter using (a) Eigen and (b) Mean templates.

Figure 6.10: P_e and P_D for $v = 1$

Figure 6.11: P_e and P_D for $v = 0.7$

Data

Power-Transform Normalised

Normalised Power-Transform

Mean	SVD	Mean	SVD	Mean	SVD

LS	Matched	LS	Matched	LS	Matched	LS	Matched	LS	Matched	LS	Matched
.0576	.0353	.0576	.0194	.0582	N/A	.0594	N/A	.0582	N/A	.0594	N/A
.9424	.9647	.9424	.9806	.9418		.9406		.9418		.9406	
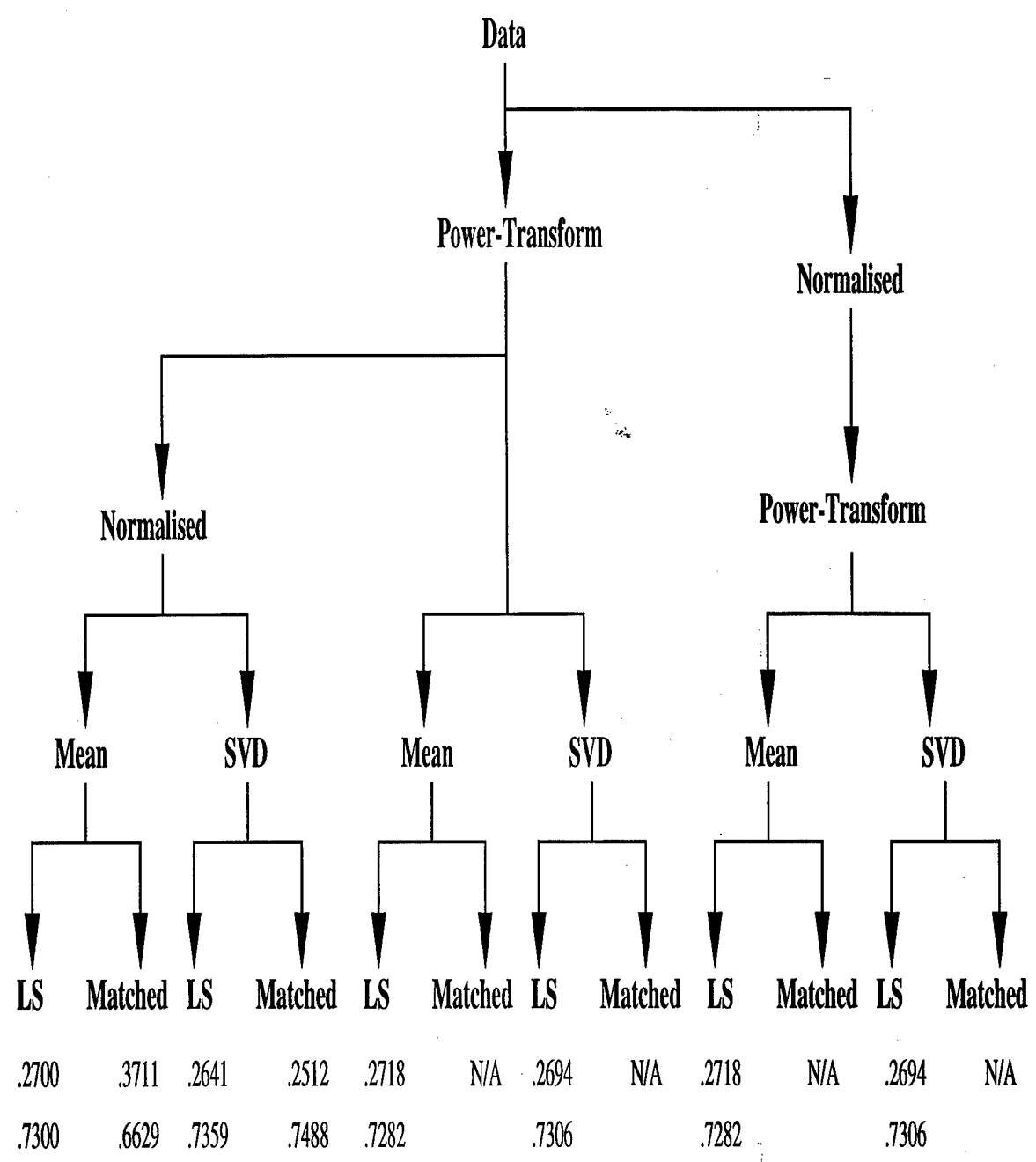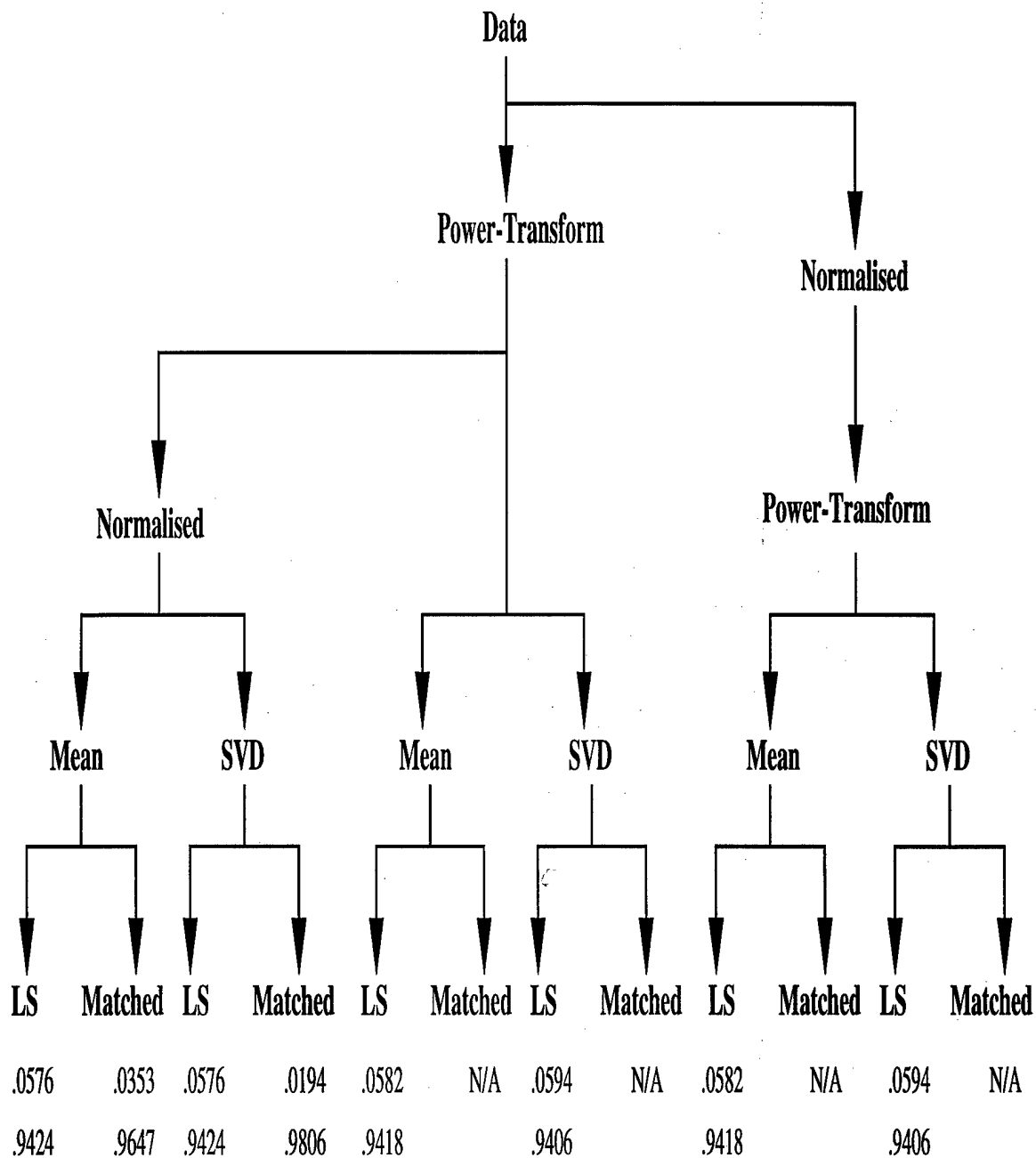
Figure 6.12: P_e and P_D for $v = 0.2$
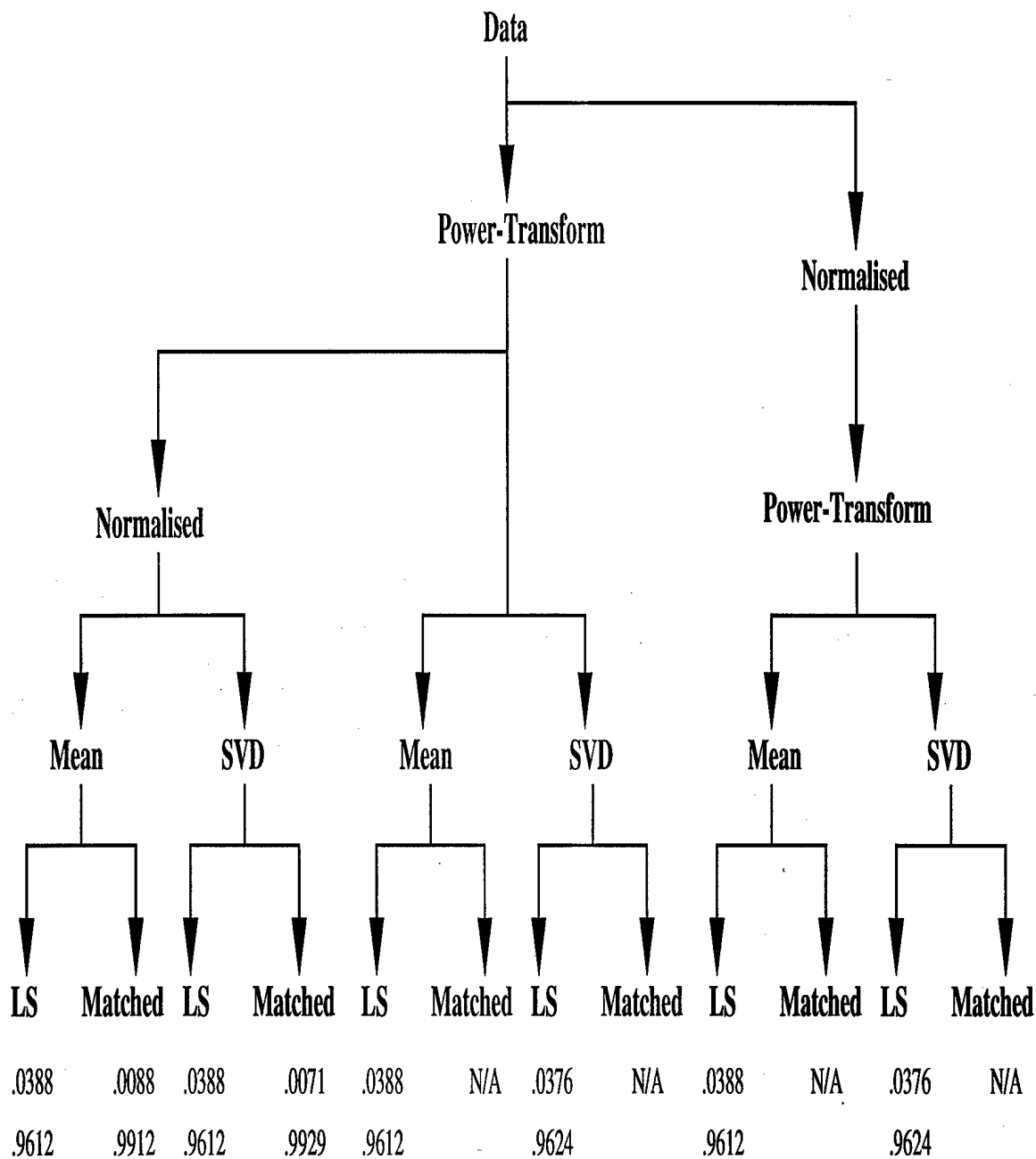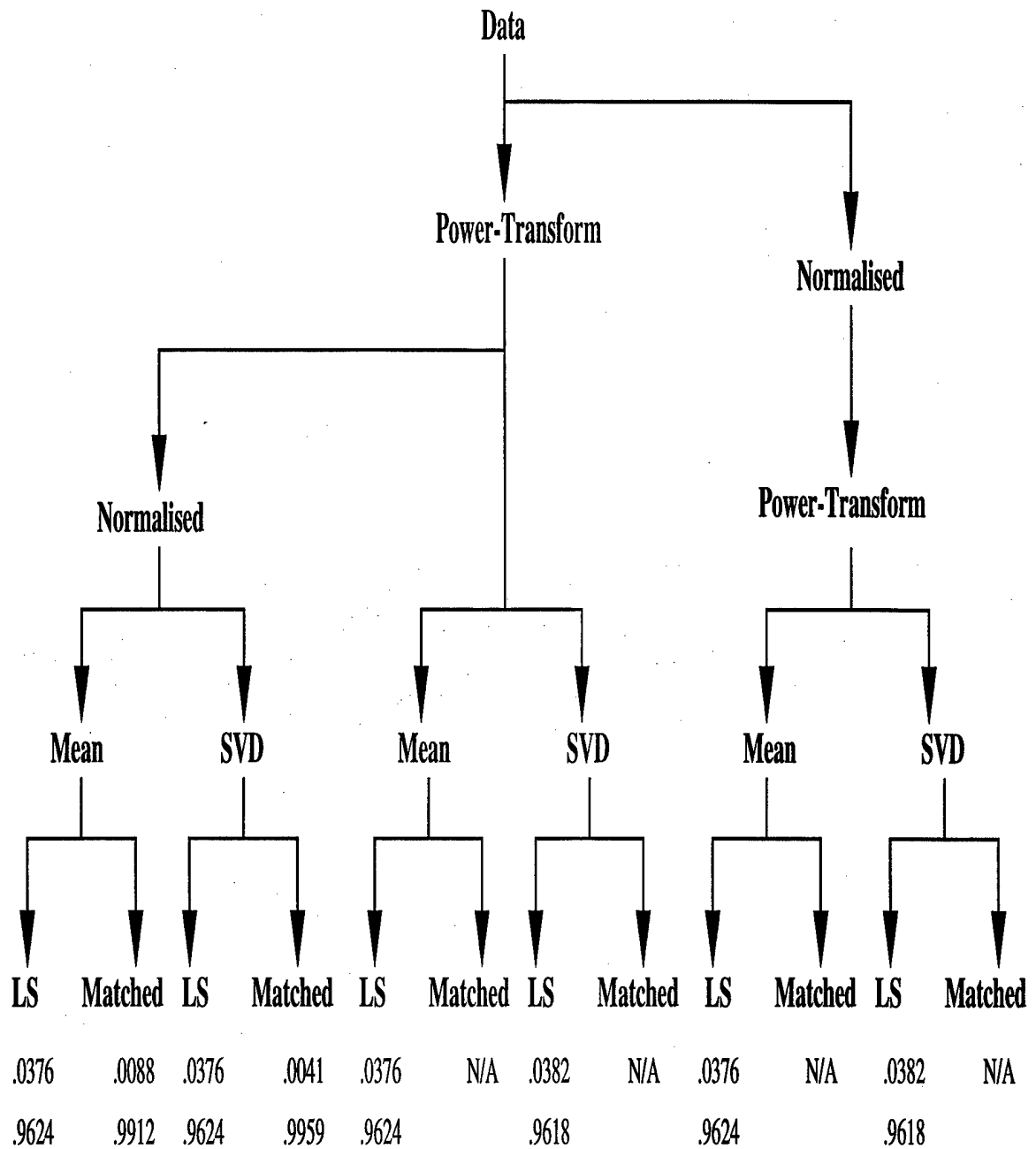
Figure 6.13: P_e and P_D for $v = 0.1$

Figure 6.14: P_e and P_D for $v = 0.08$

Chapter 7

Summary and Future Work

7.1 Conclusion

A new approach using High Range Resolution (HRR) profiles to recognize time critical military targets is considered in this project. In order to overcome the limitations of Synthetic Aperture Radar (SAR) image-based ATR in recognition of moving targets, the HRR scheme, studied as part of this project, can be used to obtain superior recognition rates. HRR-ATR also offers considerable computational savings when compared with SAR-ATR scheme. Most results described in this report were based on XPATCH database, although some results with the new MSTAR data set is also included.

This report includes details of how HRR profiles are created and pre-processed to achieve superior ATR performance. For large number of target classes with significantly large number of templates, considerable on-line processing may be necessary for classification. As a trade-off, range profiles are divided into sectors where the sector-sizes are decided based on the correlation drop between sector to sector. From sector size simulation study of XPATCH data, it was shown that a sector size of 2.5° is appropriate for limiting computation while achieving excellent ATR performance.

Many commonly known estimation and detection algorithms for ATR work best or are computationally simple for gaussian signals. HRR profiles being positive valued,

80

these tests are described in details and they show that for $v = 0.08$ is range profiles are mapped to be most gaussian-like. To verify the results of these studies, various values of Power transform were tested in ATR Simulations in Chapter 6. For the 4-targets XPATCH database, so far the highest achievable ATR efficiency was found to be about 99.5% using Eigen-templates in conjunction with Matched Filtering with Power Transformed (with a coefficient value of 0.08) and normalized profile data.

In this project we have also conducted preliminary study of effectiveness of SVD for removal of clutter from a HRR profiles as well as SAR images. It has been shown that Eigen filtering technique, *i.e.*, reconstruction after zeroing out small singular values, which correspond to noise or clutter, can be highly effective removing clutter.

7.2 Future Work

The algorithms proposed in this thesis are made with the objective to achieve high ATR/D for moving targets. At the present stage, the algorithms have been tested for stationary synthetic XPATCH database and to some extent with measured MSTAR data set. Although the HRR-ATR algorithms have been developed initially for stationary targets (XPATCH) for base-lining purposes, once moving target data is available the algorithms need to be modified and tested for those or any other database to test their effectiveness. Recent advances in superior sensor technologies and sensor simulation tools that allow wider classes of target scenarios available at the ATR developmental stage, higher resolution imaging based on super-resolution techniques [19, 18, 30], increasingly faster and superior computing hardware, and appropriate advanced ATR strategies [1] are all expected to be beneficial for achieving improved performance from the evolving ATR methodologies.

Eigen-templates as features need to be applied for Measured data and Moving Targets (MSTAR) once more datasets are made available. For measured data with

considerable presence of clutter, some form of sequential processing using more than one observation profile may be necessary. Sequential computation of eigen-vectors to extract appropriate information from observation profiles also need to be studied. Furthermore, the energy of some targets may be distributed among more than the largest singular value and more than one eigenvector may be more appropriate for template formation for some targets to achieve reasonable ATR results. The proposed eigen-filter based clutter removal technique has shown considerable promise and it needs to be studied further.

Bibliography

[1] K. Augustyn. A new approach to automatic target recognition. *IEEE Transactions on Aerospace and Electronic Systems*, 28(1):105–114, January 1992.

[2] A. Bhattacharya. On a measure of divergence between two statistical populations defined by their probability distributions. *Bulletin of Calcutta Mathematical Society*, 35:99–110, 1943.

[3] C. Bottcher and M. R. Strayer. Classical scattering theory of waves from the view point of an eigenvalue problem and application to target identification. *SPIE PROCEEDINGS*, 1960(3):425–435, April 1993.

[4] W. G. Carrara, R. S. Goodman, and R. M. Majewski. *Spotlight synthetic aperture radar : signal processing algorithms*. Boston : Artech House, 1995.

[5] R. G. Cave, P. J. Harley, and S. Quegan. Matching map features to synthetic aperture radar (sar) images using template matching. *IEEE Transactions on Geoscience and Remote Sensing*, 30:680–685, July 1992.

[6] J. C. Curlander and R. N. McDonough. *Synthetic Aperture Radar*. John Wiley & Sons, Inc., 1991.

[7] D. E. Dudgeon and R. T. Lacoss. An overview of automatic target recognition. *The Lincoln Laboratory Journal*, 6(1), 1993.

[8] H. Frank and S. C. Althoen. *Statistics : concepts and applications.* Cambridge [England] ; New York, NY, USA : Cambridge University Press, 1994.

[9] K. Fukunaga. *Introduction to Statistical pattern recognition.* Boston: Academic Press, 1990.

[10] W. W. Goj. *Synthetic Aperture Radar and Electronic Warfare.* Artech House, MA, 1993.

[11] P. E. Greenwood and M. S. Nikulin. *A guide to chi-squared testing.* New York : John Wiley & Sons, 1996.

[12] A. Haimovich. The eigencanceler: Adaptive radar by eigenanalysis methods. *IEEE Transactions on Aerospace and Electronic Systems*, 32(2):532–542, April 1996.

[13] S. A. Hovanessian. *Introduction to Synthetic Array and Imaging Radars.* Artech House, 1980.

[14] C. W. Jakowatz. *Spotlight-mode synthetic aperture radar : a signal processing approach.* Boston : Kluwer Academic Publishers, 1996.

[15] I. Jouny, F. D. Garber, and R. L. Moses. Radar target identification using the bispectrum: A comparative study. *IEEE Transactions on Aerospace and Electronic Systems*, AES-14, 3, May 1978.

[16] S. M. Kay. *Modern Spectral Estimation, Theory & Application.* Prentice Hall, Englewood Cliffs, New Jersey, 1988.

[17] J. J. Kovaly. *Synthetic Aperture Radar.* Artech House, MA, 1976.

[18] R. Kumaresan, L. L. Scharf, and A. K. Shaw. An algorithm for pole-zero modeling and spectral estimation. *IEEE Transactions on Acoustics Speech and Signal Processing*, 34:637–640, June 1986.

[19] R. Kumaresan and D. W. Tufts. Estimating the angles of arrival of multiple plane waves. *it IEEE Transactions on Aerospace and Electronic Systems*, 19(1):134–139, January 1983.

[20] J. Lee. Principal components transformation of multifrequency polarimetric sar imagery. *IEEE Transactions on Geoscience and Remote Sensing*, 30, July 1992.

[21] J. Li and E. G. Zelnio. Target detection with synthetic aperture radar. *IEEE Transactions on Aerospace and Electronic Systems*, 32, April 1996.

[22] L. M. Novak, S. D. Halversen, G. J. Owirka, and M. Hiett. Effects of polarization and resolution on the performance of a sar automatic target recognition system. *The Lincoln Laboratory Journal*, 8(1), 1995.

[23] A Papoulis. *Probability, Random Variables, and Stochastic Processes*. McGraw-Hill, New York, 1965.

[24] D. Povejsil, R. Raven, and P. Waterman. *Airborne Radar*. D. Van Nostrand, Princeton, NJ, 1961.

[25] T. S. Rao and M.M. Gabr. *An Introduction to Bispectral Analysis and Bilinear Time Series Models*. Springer-Verlag, New York Berlin Heidelberg Tokyo, 1984.

[26] L. R. Rabiner S. E. Levinson and M. M. Sondhi. An introduction to the application of the theory of probabilistic functions of a markov process to automatic speech recognition. *Bell Systems Technical Journal*, 62:1035, 1983.

[27] D. C. Scheler. *MTI Radar*. Artech House, INC., 1980.

[28] D. C. Scheler. *MTI and Pulsed Doppler Radar*. AIL Systems, INC., 1991.

[29] D. C. Schleher. *MTI and Pulsed Doppler Radar*. Artech House, MA, 1991.

[30] R. O. Schmidt. Multiple emitter location and signal parameter estimation. *Proceedings of RADC Spectral Estimation Workshop*, pages 243–258, 1979.

[31] K. S. Shanmugan and A. M. Breipohl. *Random Signals, Detection Estimation and Data Analysis*. John Wiley & Sons, 1988.

[32] A. K. Shaw. Maximum likelihood estimation of multiple frequencies with constraints to guarantee unit circle roots. *IEEE Transactions on Signal Processing*, 43(3):796–799, March 1995.

[33] A. K. Shaw and W. Xia. Minimum-norm method without eigendecomposition. *IEEE Signal Processing Letters*, 1(1):12–14, January 1994.

[34] M. D. Srinath, P. K. Rajasekaran, and R. Vishwanathan. *Introduction to Statistical Signal Processing with Applications*. Prentice-Hall Inc., Englewood cliffs, New Jersey 07632, 1996.

[35] G. Stimson. *Introduction to Airborne Radar*. Hughes Aircraft Company, El Segundo, CA, 1983.

[36] C. W. Therrien. A sequential approach to target discrimination. *IEEE Transactions on Aerospace and Electronic Systems*, AES-14, 3, May 1978.

[37] C. W. Therrien. *Decision, estimation and classification : an introduction to pattern recognition and related topics*. New York : Wiley, 1989.

[38] D. W. Tufts and R. Kumaresan. Frequency estimation of multiple sinusoids : Making linear prediction perform like maximum likelihood. *Proceedings of the IEEE*, 70:975–989, September 1982.

[39] J. G. Verly and R. L. Delanoy. Model-based automatic target recognition (atr) system for forwardlooking groundbased and airborne imaging laser radars (ladar). *Proceedings of the IEEE*, 84(2), February 1996.

[40] D. R. Wehner. *High Resolution Radar*. Artech House, MA, 1987.

[41] S. Worrell. Synthetic aperture radar and signal processing. *An unclassified presentation*, 1995.

[42] S. Worrell. Air to ground automatic target recognition. *An unclassified report*, 1996.